The Astrophysical Journal, 677:12–26, 2008 April 10

REIONIZATION AND GALAXY EVOLUTION PROBED BY $z = 7$ Lyα EMITTERS[1]

Kazuaki Ota,[2] Masanori Iye,[3,4,5] Nobunari Kashikawa,[3,5] Kazuhiro Shimasaku,[4] Masakazu Kobayashi,[6] Tomonori Totani,[6] Masahiro Nagashima,[7] Tomoki Morokuma,[3] Hisanori Furusawa,[8] Takashi Hattori,[8] Yuichi Matsuda,[6] Tetsuya Hashimoto,[4] and Masami Ouchi[9,10]

Received 2007 July 10; accepted 2007 December 29

ABSTRACT

We have performed narrowband NB973 (bandwidth 200 Å centered at 9755 Å) imaging of the Subaru Deep Field (SDF) and found two $z = 7$ Lyα emitter (LAE) candidates down to NB973 = 24.9. Carrying out deep follow-up spectroscopy, we identified one of them as a real $z = 6.96$ LAE. This has established a new redshift record, showing that galaxy formation was in progress just 750 Myr after the big bang. Meanwhile, the Lyα line luminosity function of LAEs is known to decline from $z = 5.7$ to 6.6 in the SDF; L^* at $z = 6.6$ is 40%–60% that at $z = 5.7$. We also confirm that the number density of $z = 7$ LAEs is only 17% of the density at $z = 6.6$ comparing the latest SDF LAE samples. This series of significant decreases in LAE density with increasing redshift could be the result of galaxy evolution during these epochs. However, using the UV continuum luminosity functions of LAEs and Lyman break galaxies, and a LAE evolution model based on hierarchical clustering, we find that galaxy evolution alone cannot entirely explain the decrease in density. This extra density deficit might reflect the attenuation of the Lyα photons from LAEs by the neutral hydrogen possibly left at the last stage of cosmic reionization at $z \sim 6$–7.

Subject headings: cosmology: observations — early universe — galaxies: evolution — galaxies: high-redshift

1. INTRODUCTION

Investigating high-redshift galaxies, as well as other distant objects in the early universe, especially within the first 1 Gyr after the big bang, has been the key to understanding how galaxies formed and evolved, probing their star formation histories, and constraining the epoch of cosmic reionization. The latest measurements of the polarization of the cosmic microwave background (CMB) by *Wilkinson Microwave Anisotropy Probe* (*WMAP*) constrained the optical depth to electron scattering during reionization, and suggest that the average redshift of reionization was $z = 10.9^{+2.7}_{-2.3}$ (Spergel et al. 2007; Page et al. 2007). Gunn-Peterson (GP) troughs (Gunn & Peterson 1965) in $z \sim 6$ quasar spectra imply that reionization ended at $z \sim 6$, with an estimated fraction of intergalactic medium (IGM) neutral hydrogen $x_{\rm H\,I}^{z\sim6.2} \sim 0.01$–$0.04$ (Fan et al. 2006). Moreover, a spectral modeling analysis of a $z \sim 6.3$ gamma-ray burst (GRB) shows that the universe seems to have been largely reionized at $z \sim 6.3$, with $x_{\rm H\,I}^{z\sim6.3} = 0$ and an upper limit of $x_{\rm H\,I}^{z\sim6.3} < 0.17$–$0.6$, which suggests only some reasonable amount of neutral gas in the GRB host galaxy (Totani et al. 2006).

Another probe of reionization is Lyα emitters (LAEs), young galaxies in the distant universe showing in their spectra redshifted Lyα emission from their interstellar gas illuminated by massive stars. The observed Lyα line luminosity function (Lyα LF) is expected to decline beyond $z \sim 6$, where reionization is thought to have completed as the increasing fraction of IGM neutral hydrogen absorbs or scatters the Lyα photons from young galaxies (Haiman & Spaans 1999; Rhoads & Malhotra 2001; Hu et al. 2002). Nevertheless, recent LAE surveys show that Lyα LF seems not to change from $z = 3$ to 5.7 (Ouchi et al. 2003, 2007; Ajiki et al. 2003; Tran et al. 2004; van Breukelen et al. 2005). For the earlier epoch, Malhotra & Rhoads (2004) suggest that Lyα LF does not evolve between $z = 5.7$ and 6.6. Their sample may be somewhat biased, since it consists of several LAE subsamples taken from various surveys with different selection criteria, analysis methods, sky areas, survey volumes, and depths, in order to compile as large a sample as possible.

On the other hand, the Subaru Deep Field (SDF; Kashikawa et al. 2004) surveys have tried to keep all these factors as consistent as possible for different redshifts, surveying exceptionally large volumes and taking large LAE samples at $z = 4.8$, 5.7, and 6.6. Their latest survey has for the first time confirmed that the Lyα LF declines as $L^*_{z=6.6} \sim (0.4$–$0.6)L^*_{z=5.7}$ from $z = 5.7$ to 6.6 even after correcting for cosmic variance (Kashikawa et al. 2006b). From this decline of the LF, they estimated the upper limit of the neutral fraction at $z = 6.6$ to be $0 \leq x_{\rm H\,I}^{z=6.6} \leq 0.45$. If the neutral IGM remains at the ~50% level at $z = 6.6$, this constraint supports late reionization and contradicts the *WMAP* result. The decline of Lyα LF at $z = 5.7$–6.6 could also be ascribed to evolution of the LAE population itself.

Meanwhile, the ionized fraction $x_i < 1$ and the morphology of H II regions during patchy reionization would modulate the observed distribution of LAEs and enhance their observed clustering (Furlanetto et al. 2006; McQuinn et al. 2007). McQuinn et al. (2007) investigated the angular correlation function of the SDF photometric sample of $z = 6.6$ LAEs obtained by Kashikawa

[1] Based on data collected at Subaru Telescope, which is operated by National Astronomical Observatory of Japan.

[2] Cosmic Radiation Laboratory, RIKEN, 2-1 Hirosawa, Wako-shi, Saitama 351-0198, Japan; kz_ota@crab.riken.jp.
[3] National Astronomical Observatory of Japan, 2-21-1 Osawa, Mitaka, Tokyo, 181-8588, Japan.
[4] Department of Astronomy, Graduate School of Science, University of Tokyo, 7-3-1 Hongo, Bunkyo-ku, Tokyo 113-0033, Japan.
[5] The Graduate University for Advanced Studies, 2-21-1 Osawa, Mitaka, Tokyo, 181-8588, Japan.
[6] Department of Astronomy, Kyoto University, Sakyo-ku, Kyoto 606-8502, Japan.
[7] Faculty of Education, Nagasaki University, 1-14 Bunkyo-machi, Nagasaki 852-8521, Japan.
[8] Subaru Telescope, 650 North A'ohoku Place, Hilo, HI 96720.
[9] Space Telescope Science Institute, 3700 San Martin Drive, Baltimore, MD 21218.
[10] Hubble Fellow.

et al. (2006b) and suggest that the universe is fully ionized at $z = 6.6$, with a mean volume ionized fraction of $\bar{x}_i \sim 1$. McQuinn et al. (2007) also pointed out the difficulty of distinguishing the effects of the evolution of the LAE population on the Lyα LF from the effects of reionization.

LFs of high-z galaxies also tell us about galaxy evolution itself, in terms of how many galaxies existed at each luminosity and epoch in the history of the universe, and how this has changed with cosmic time. To obtain this information at high redshifts, LFs of Lyman break galaxies (LBGs) and LAEs have been observed. Ultraviolet continuum luminosity functions (UVLFs) of LBGs have been investigated from $z \sim 3$ to $z \sim 7$ and found to decline as redshift increases (Lehnert & Bremer 2003; Ouchi et al. 2004; Bouwens et al. 2006; Yoshida et al. 2006; Bouwens & Illingworth 2006). Since the UV continuum redder than 1216 Å is not attenuated by neutral IGM hydrogen, and if dust extinction is precisely corrected, the decline of UVLF reflects the evolution of galaxies.

One recently observed example of this is a large decline in the UVLF of dropout galaxies at $6 < z \lesssim 7$–8, which is considered to be a clear sign of galaxy evolution over these redshifts (Bouwens & Illingworth 2006). They conclude that very luminous galaxies are quite rare at $z = 7$–8. On the other hand, the UVLF of LAEs was confirmed not to evolve at $z \sim 3$–5 (Ouchi et al. 2003). In addition, studying LAEs in an even wider sky region, $\sim$1.0 deg^2 of the Subaru/*XMM-Newton* Deep Survey (SXDS) field, Ouchi et al. (2007) found that the UVLF of LAEs increases from $z \sim 3$–4 to 5.7, while their Lyα LF remains unchanged at these redshifts, suggesting that the fraction of UV-bright LAEs increases at $z = 5.7$. Furthermore, no evolution was observed in the LAE UVLF from $z = 5.7$ to 6.6, while the Lyα LF of LAEs evolves between these epochs in the latest SDF survey (Kashikawa et al. 2006b). This implies that LAEs themselves do not significantly evolve from $z = 6.6$ to 5.7, and the decline of the Lyα LF might reflect the effects of reionization. However, we do not know if this trend of the Lyα LF and UVLF of LAEs continues from even earlier epochs. In other words, it is not clear whether the LAE population evolves from $z > 6.6$ as LBGs do, but the neutral IGM fraction increases to suppress the Lyα LF more severely beyond $z = 6.6$. Moreover, the existence of galaxies at $z > 6.6$ has not yet been confirmed by spectroscopy, although several photometric candidates have been found. These questions can be addressed by observing LAEs and their LFs at $z > 6.6$. Investigating their changes over longer a cosmic time interval, we can constrain the galaxy evolution and reionization more tightly.

One possible method of detecting $z > 6.6$ LAEs is a narrowband filter imaging in the infrared. However, beyond the redward limit of CCD sensitivity, the large-format mosaicking advantages of infrared arrays are not yet available, and observations of high-redshift LAEs is limited to a small survey volume. Although recent infrared detectors have achieved extremely high sensitivities, surveys cannot avoid large uncertainty due to cosmic variance. Therefore, we carried out a narrowband survey of $z = 7$ LAEs using the final window of OH airglow at the very edge of the optical regime still accessible with CCDs of the Subaru Prime Focus Camera (Suprime-Cam; Miyazaki et al. 2002), having a superb wide field of view, $34' \times 27'$. We chose the wavelength region 9655–9855 Å, open to the highest redshift optical narrowband survey. Although this might not be considered quite an adequate window, since there are several OH lines in the region, the estimated fraction of the sky counts coming from OH lines in the window is not prohibitively large (only $\sim$4.3 photons s^{-1} Å^{-1} arcsec^{-2} m^{-2}), and we actually succeeded in making a narrowband filter, NB973, covering this wavelength region. This range corresponds to a redshift of $6.9 \leq z \leq 7.1$ for LAEs.

To discover such extremely high redshift LAEs and make a sample of them as consistent as possible with samples of $z = 5.7$ and 6.6 LAEs obtained by Shimasaku et al. (2006) and Kashikawa et al. (2006b), we targeted the same field, SDF, using the 8.2 m Subaru Telescope/Suprime-Cam. Brief preliminary results were reported in Iye et al. (2006). In this survey, we successfully spectroscopically confirmed a $z = 6.96$ LAE, and observed that the number density of $z = 7$ LAE further declines from $z = 6.6$ by a factor of 0.18–0.36, suggesting that the neutral hydrogen might increase between these epochs. However, we do not know whether there was any evolution of the LAE population itself from $z = 7$ to 6.6, and the density deficit might also arise from such a galaxy evolution.

In this paper, we present the methods and results of our photometric and spectroscopic surveys for $z = 7$ LAEs, which were not fully covered in Iye et al. (2006), and try to draw out as much useful information as possible about the epoch of reionization and the LAE galaxy evolution from our results, combined with the most recent high-redshift galaxy surveys and a LAE evolution model based on hierarchical clustering. We first describe the properties of our narrowband filter NB973 and imaging observation in § 2. Then, selection criteria for $z = 7$ LAE candidates based on narrow- and broadband images are derived in detail and their photometric properties are analyzed in § 3. In § 4, we explain the results of our follow-up spectroscopy on the selected candidates and their spectroscopic properties. In § 5, we compare Lyα and UV LFs of $z = 7$ LAEs with those of $z = 5.7$ and 6.6 LAEs derived from the latest samples obtained by the SDF LAE surveys (Shimasaku et al. 2006; Kashikawa et al. 2006b), and discuss what implications the results have for cosmic reionization and galaxy evolution. In addition, various possibilities for LAE galaxy evolution at $z = 5.7$–7 are examined observationally and theoretically. In the last section, we conclude and summarize our results. Throughout, we adapt a concordance cosmology with $\Omega_m = 0.3$, $\Omega_\Lambda = 0.7$, $h = 0.7$, and AB magnitudes with $2''$ diameter aperture, unless otherwise specified.

2. IMAGING OBSERVATION

We developed a narrowband filter, NB973, designed to cover the last optical window of OH airglow, centered at 9755 Å with $\Delta\lambda_{\rm FWHM} \sim 200$ Å, corresponding to Lyα emission at $6.9 \leq z \leq 7.1$ (Iye et al. 2006). The design and fabrication of such a narrowband filter was not a simple issue for Suprime-Cam, which uses a fast-converging f/1.83 beam whose incident angle varies with position in the field of view. The mixture of light with different incident angles severely degrades the resulting transmission characteristics of the narrowband filter from our target design. To obtain the desired performance, complying with the filter specification for our scientific requirements, we employed a combination of three filters glued together: a color cut-glass filter RG780 with antireflection coating, a narrow-bandpass multilayer coating filter, and another multilayer coating filter for preventing red leak. One year before starting on the NB973 filter for Suprime-Cam, we made another filter, NB980 (bandwidth $\sim$100 Å centered at $\sim$9800 Å), for use in the parallel beam section of the Faint Object Camera and Spectrograph (FOCAS; Kashikawa et al. 2002) on Subaru, to demonstrate the feasibility of narrowband imaging at this last OH window. During the prefabrication of NB980, manufacturing errors in controlling the thickness of thin film layers were evaluated. The multilayer thin-film coating design for NB973 was then optimized so that

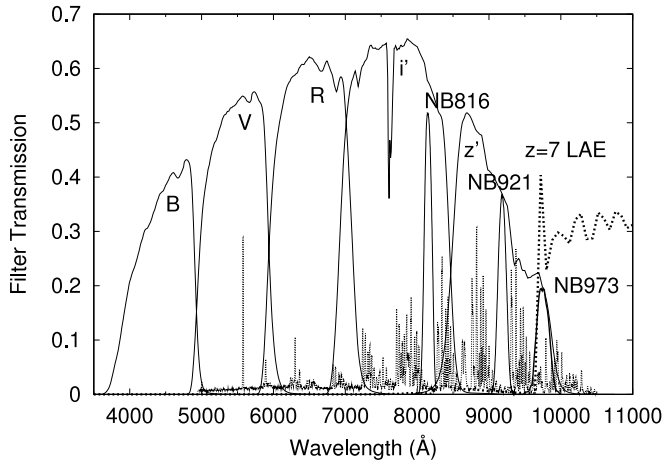

FIG. 1.—Filter transmission of the Suprime-Cam broadbands (*BVRi′z′*; *thin solid curves*) and narrowbands (NB816, NB921; *thin solid curves*, and NB973; *thick solid curve*) used for our photometry. The OH night sky lines are also overplotted with a thin dashed curve. Our NB973 filter is ∼1.5 times wider in FWHM than other narrowband filters and includes some OH lines in its bandpass. Thick dashed line shows the model spectral energy distribution (SED) of our target, a $z = 7$ LAE, obtained using a stellar population synthesis model (Bruzual & Charlot 2003) with a metallicity of $Z = Z_{\odot} = 0.02$, an age of $t = 1$ Gyr, Salpeter initial mass function with lower and upper mass cutoffs of $m_L = 0.1\,M_{\odot}$ and $m_U = 100\,M_{\odot}$, and exponentially decaying star formation history for $\tau = 1$ Gyr, and with a Lyα emission of the rest frame equivalent width of 50 Å. The NB973 flux of a $z = 7$ LAE is expected to show a strong excess with respect to its z' band flux and should not be detected in other shortward wave bands.

the resulting transmitting properties are relatively robust to inevitable manufacturing errors to control the thickness of each thin layer. The measured transmission curve of the final NB973 filter actually used in the present survey, as well as other filters used for color selection of $z = 7$ LAE candidates, are shown in Figure 1.

Our target sky region is the SDF ($13^{\rm h}24^{\rm m}21.^{\rm s}4$, $-27^{\circ}29'23''$ [J2000], ∼876 arcmin^2; Kashikawa et al. 2004), a blank field in which $z = 5.7$ and 6.6 LAE surveys have been also carried out (Shimasaku et al. 2006; Kashikawa et al. 2006b). Deep broadband *BVRi′z′* and narrowband NB816 ($\lambda_c = 8160$ Å, $\Delta\lambda_{\rm FWHM} = 120$ Å) and NB921 ($\lambda_c = 9196$ Å, $\Delta\lambda_{\rm FWHM} = 132$ Å) filter images were taken by the SDF project. All the images were convolved to have a common seeing size of $0.98''$. Limiting magnitudes in a $2''$ aperture at 3 σ are $(B, V, R, i', z', {\rm NB816}, {\rm NB921}) = (28.45, 27.74, 27.80, 27.43, 26.62, 26.63, 26.54)$. Transmissions of these filters, including CCD quantum efficiency, the reflection ratio of the telescope prime mirror, correction for the prime focus optics, and transmission to the atmosphere (airmass sec $z = 1.2$), are also shown in Figure 1.

Our NB973 image of the SDF was taken with Suprime-Cam mounted on the Subaru Telescope on 2005 March 16 and 17. These two nights were photometric, with good seeing of $\sim 0.5''$–$0.8''$. The total integration time is 15 hr. We have reduced the NB973 image frames using the software SDFRED (Ouchi et al. 2004; Yagi et al. 2002) in the same manner as in Kashikawa et al. (2004). The NB973 image frames were dithered in a similar way as the SDF project did for other wave bands when they were taken. The combined NB973 image removed the slight fringing caused by OH airglow that appeared in some image frames. The loss of survey area due to this dithering is only ∼5%. The seeing size of the combined image was $0.78''$ and convolved to $0.98''$, which is the common seeing size of the images of other wave bands, for the purpose of photometry. Spectrophotometric standard stars Feige 34 and Hz 44 (Oke 1990) were imaged during the observation to calibrate the photometric zero point of the stacked image, which is NB973= 32.03. The limiting magnitude reached NB973$\leq$ 24.9 at 5 σ, with 15 hr integration.

3. PHOTOMETRIC ANALYSIS

3.1. *Photometry*

After obtaining the stacked NB973 image, we conducted photometric analysis, making an object catalog. Source detection and photometry were carried out with SExtractor software version 2.2.2 (Bertin & Arnouts 1996). The pixel size of the Suprime-Cam CCDs is $0.202''$ pixel^{-1}. We considered any area larger than contiguous 5 pixels with a flux (mag arcsec^{-2}) greater than 2 σ to be an object. Object detection was first made in the NB973 image, and then photometry was done in the images of other wave bands using the double-imaging mode. The $2''$ diameter aperture magnitudes of detected objects were measured with the `MAG_APER` parameter, and total magnitudes with `MAG_AUTO`. Low-quality regions of CCDs, bright stellar halos, saturated CCD blooming, and pixels of spiky abnormally high or low flux counts were masked in the SDF images of all wave bands, using the official program code[11] provided by the SDF team (Kashikawa et al. 2004). The final effective area of the SDF image is 876 arcmin^2. The comoving distance along the line of sight corresponding to the redshift range $6.94 \leq z \leq 7.11$ for LAEs covered by the NB973 filter was 58 Mpc. Therefore, we have surveyed a total of 3.2×10^5 Mpc^3 volume using NB973 images. Then, the final object catalog was constructed, detecting 41,533 objects down to NB973 $\leq$ 24.9 (5 σ).

3.2. *Detection Completeness*

To understand how reliable our source detections are down to the limiting magnitude of NB973 $\leq$ 24.9, we measured the detection completeness of our photometry with the NB973 image. First, all the objects that satisfy our source detection criterion were removed from the NB973 image using SExtractor. Then, the `starlist` task in the `artdata` package of IRAF[12] was used to create a sample star list of about 20,000 artificial objects with a random but uniform spatial and luminosity distribution, ranging from NB973= 20 to 25 mag. Next, using the `mkobject` task of IRAF, these artificial objects were spread over the NB973 image, avoiding the masked regions of the SDF and the locations close to the previously removed real objects with distances shorter than 3/2 of their FWHM. After this, SExtractor was run for source detection in exactly the same way as our actual photometry. Finally, we calculated the ratio of the number of detected artificial objects to that of created ones to obtain the detection completeness. We repeated this procedure five times and averaged the obtained completenesses. The result is shown in Figure 2. The completeness at our detection limit of NB973= 24.9 is ∼76%. The completeness was corrected when the number and luminosity densities of $z = 7$ LAEs were calculated in § 5.

We evaluated the completeness in the same way as Shimasaku et al. (2006) and Kashikawa et al. (2006b) did for the detection completeness of $z = 5.7$ and $z = 6.6$ LAEs, for consistency. However, in actual observations, some $z = 7$ galaxies will lie behind brighter sources at lower redshifts, and thus the completeness correction will be artificially small. The fractions that are thus obscured can be included in the completeness estimate by simply

[11] Available from http://step.mtk.nao.ac.jp/sdf/data/.

[12] IRAF is distributed by the National Optical Astronomy Observatories, which are operated by the Association of Universities for Research in Astronomy, Inc., under cooperative agreement with the National Science Foundation.

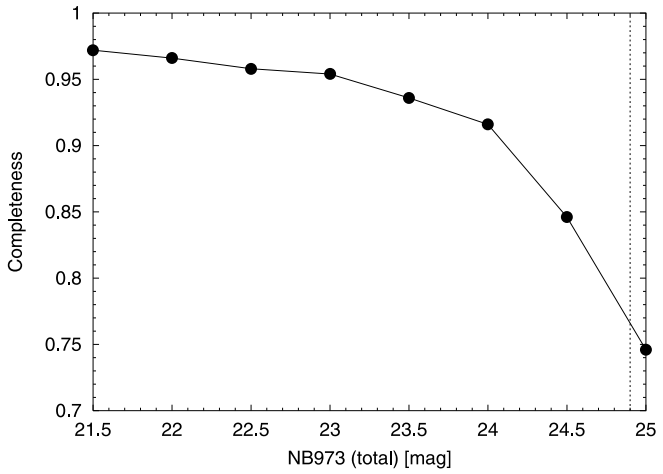

FIG. 2.—Detection completeness of our NB973 image of the SDF, calculated for every 0.5 mag bin. The dashed line shows our survey limit. The completeness does not reach 1.0 even for the objects with bright magnitudes, since blended or overlapped objects tend to be counted as one object by SExtractor. The completeness is corrected when the number and luminosity densities of $z = 7$ LAE are calculated in § 5.

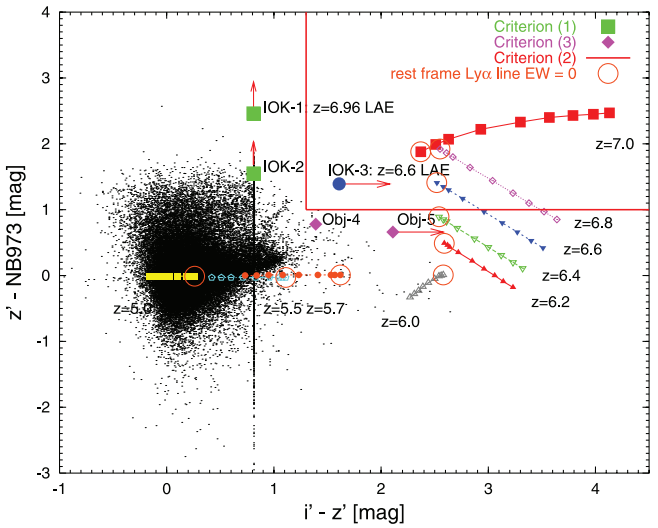

FIG. 3.—$z' - \mathrm{NB973}$ vs. $i' - z'$ plot of the objects with NB973 ≤ 24.9 (total magnitude) detected in the SDF (*black dots*). The upper right rectangle surrounded by the solid line indicates the color selection criterion (2). Colors and selection criteria of IOK-1, IOK-2 (*larger green filled squares*), and IOK-3 (*larger blue filled circle*), as well as Obj-4 and Obj-5 (*filled diamonds*) are also shown and labeled. The colors of model LAEs at $z = 5.0$–7.0 with rest-frame Lyα line equivalent widths of $\mathrm{EW_0(Ly}\alpha) = 0$, 10, 20, 50, 100, 150, 200, 250, and 300 Å are shown by other symbols and lines, as labeled on the figure. Each point with $\mathrm{EW_0(Ly}\alpha) = 0$, which is the first point in each sequence, is circled. The model $z = 7$ LAEs are shown by smaller red filled squares with a solid line. All the i' and z' magnitudes fainter than their 2 σ limits were replaced by the 2 σ values in the application of the color-selection criteria, and are shown by arrows in this diagram.

adding artificial sources to the original image without masking out anything and without any exclusion zones in the placement of artificial sources. We also calculated our detection completeness in this way to see how different it is from the original completeness evaluation. As expected, the completeness we calculated this time is slightly smaller. However, the difference is a factor of only 1.1–1.3 over NB973= 20–25, and it does not change the evaluation of LAE number and luminosity densities much. Hence, for our subsequent analyses, we use the original completeness calculated in the same way as done for $z = 5.7$ and $z = 6.5$ LAEs, for consistency.

3.3. *Colors and Selection Criteria of $z = 7$ LAEs*

To isolate $z = 7$ LAEs from other objects, we investigated their expected colors and derived candidate selection criteria. We generated model spectra of LAEs at redshifts ranging from $z = 5$ to 7, with rest-frame Lyα line equivalent width $\mathrm{EW_0(Ly}\alpha)$ varying from 0 to 300 Å, as follows. First, we created a spectral energy distribution (SED) of a starburst galaxy using a stellar population synthesis model, GALAXEV (Bruzual & Charlot 2003), with a metallicity of $Z = Z_\odot = 0.02$, an age of $t = 1$ Gyr, a Salpeter initial mass function with lower and upper mass cutoffs of $m_L = 0.1\ M_\odot$ and $m_U = 100\ M_\odot$, and an exponentially decaying star formation history for $\tau = 1$ Gyr. These parameters were chosen to be the same as those used to generate model $z = 6.6$ LAEs in Taniguchi et al. (2005), for consistency. Although recent observational studies show that LAEs seem to be much younger than the 1 Gyr age and/or 1 Gyr star formation decay time, and $z = 4.5$ LAEs seem to have dust extinction (Gawiser et al. 2006; Pirzkal et al. 2007; Finkelstein et al. 2008), we did not consider the effects of dust on the SED, since the two issues have opposite effects on the broadband colors of the LAEs, and this does not have a major effect on the LAE selection criteria. Then, the SED was redshifted to $z = 5.0$, 5.5, 5.7,. . ., and 7.0, and Lyα absorption by IGM was applied to it, using the prescription of Madau (1995). Finally, the flux of a Lyα emission line with $\mathrm{EW_0(Ly}\alpha) = 0$, 10, 20, 50, 100, 150, 200, 250, or 300 Å was added to the SED at $(1 + z)1216$ Å. We did not assume any specific line profile or velocity dispersion of Lyα emission. Instead, we simply added 1/2 of the total line flux value, assuming that the blue half of the Lyα line is absorbed by the IGM. An example of a model spectrum of a $z = 7$ LAE is shown in Figure 1.

Colors of these model LAEs were calculated using their SEDs and the transmission curves of the Suprime-Cam broadband and NB973 filters, and plotted in the two-color diagram of $z' - \mathrm{NB973}$ vs. $i' - z'$ shown in Figure 3. As clearly seen in the diagram, a $z = 7$ LAE is expected to produce significant flux excess in NB973 versus z'. However, it should be also noted that NB973 bandpass overlaps with the wavelength range at the longward edge of z' band. This would allow LAEs and LBGs at even lower redshifts, $z = 6.2$–6.8, to cause the NB973 flux excess with respect to z' band, if such galaxies have bright and steep UV continua. In fact, such objects were detected in our photometry. Their images and photometric properties are shown and described in Figure 4 and § 3.4. From these lower redshift galaxies, $z = 6.5$–6.6 LAEs can be removed by requiring no detection in the narrowband filter NB921 image, whose bandpass corresponds to the Lyα emissions at this redshift range (Kodaira et al. 2003; Taniguchi et al. 2005; Kashikawa et al. 2006b). Hence, we classified NB973-excess objects with NB973 ≤ 24.9 (5 σ, 2″ aperture), which includes our target $z = 7$ LAEs, into following two categories based on $z' - \mathrm{NB973}$ color:

1. $z = 6.9$–7.1 LAEs.—B, V, R, i', NB816, z', NB921 $< 3\ \sigma$
2. $z = 6.7$–7.1 LBGs.—B, V, R, NB816, NB921 $< 3\ \sigma$, $i' - z' > 1.3$, $z' - \mathrm{NB973} > 1.0$,

where B, V, R, i', NB816, z', and NB921 fluxes were measured in total magnitudes, while $i' - z'$ and $z' - \mathrm{NB973}$ colors in 2″ aperture magnitudes. All the i' and z' aperture magnitudes fainter than 27.87 and 27.06 (2 σ limits), respectively, were replaced by these values in the application of criterion (2). Since the flux of a LAE shortward of Lyα emission should be absorbed by the IGM, no detections (<3 σ) in B, V, R, NB816, and NB921

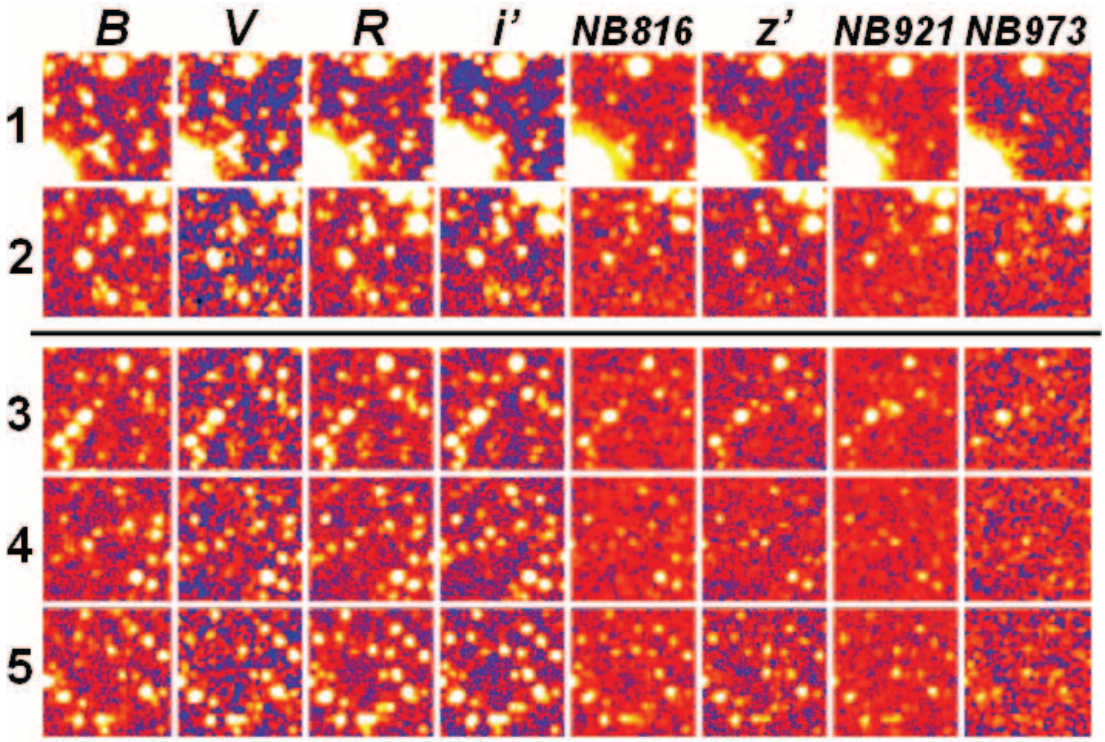

FIG. 4.—Multi-wave-band images of IOK-1, IOK-2, and IOK-3 as well as NB973–3 σ excess objects, Obj-4 and Obj-5 (labeled 1, 2, 3, 4, and 5, respectively). IOK-1, a $z = 6.96$ LAE, and IOK-2 are clearly detected only in NB973. IOK-3, a $z = 6.6$ LAE identified by Kashikawa et al. (2006b), shows a significant excess in both NB921 and NB973 against z' at the same time, but is obviously brighter in NB921. Obj-4 is seen in all the narrow bands, and the i' and z' bands, while Obj-5 is detected in z', NB921, and NB973. Both objects show 3 σ excess in $z' -$ NB973, but no excess in NB816 (bandpass for $z = 5.65$–5.75 LAEs) or NB921 (bandpass for $z = 6.5$–6.6 LAEs), and thus could be either $z = 6.2$–6.4 galaxies, low-z EROs, or late-type dwarf stars.

with either red $i' - z' > 1.3$ color or no detections in i' and z' were imposed as a part of the criteria. This can help eliminate interlopers such as L/M/T type dwarf stars and lower redshift galaxies with other types of emission lines (e.g., Hβ, [O III], [O II], Hα, [S II], and so on). Criterion (1) also implies that the robust $z = 7$ LAE candidates should show significant excess in NB973 over z' and NB921, $z' -$ NB973 > 1.72 and NB921 $-$ NB973 > 1.64.

Note that the color selection criteria (1) and (2) are slightly different from those in Iye et al. (2006) in that here we include null detections in NB816 and NB921 whose bandpasses correspond to Lyα emission at $z = 5.65$–5.75 and 6.5–6.6, respectively, to make the criteria more reliable and secure. In fact, the object IOK-3 detected by Iye et al. (2006) satisfied the criteria (1) and (2) simultaneously except for NB921 < 3 σ, and was spectroscopically identified as a $z = 6.6$ LAE by Kashikawa et al. (2006b).

This time, we found only one object satisfying criterion (1) (hereafter referred to as IOK-1, as in Iye et al. 2006), and none met criterion (2). In order not to miss faint and diffuse $z = 7$ LAEs such as Lyα blobs having extended shapes with fairly bright cores but NB973 > 24.9 (2″ aperture magnitude), we also loosened our detection limit cutoff, adopting NB973 ≤ 24.9 (total magnitude) as another limiting magnitude. This increased the number of objects satisfying criterion (1) by 17, but still no objects met (2).

However, this sample might be contaminated by some spurious objects, such as sky residuals and noise due to fringing, which might not have been removed perfectly at the time of image reduction. Hence, we visually inspected all the broadband and narrowband images of each color-selected object and only kept those appearing to have condensed and relatively bright cores, excluding those having only diffuse, faint shapes with no cores. More specifically, we removed objects that looked apparently artificial, such as connected bad pixels, tails of saturated pixels from bright stars, and noise of discrete dismembered shapes or pieces of disconnected pixels with fairly large fluxes. As a result, we were left with one object (hereafter called IOK-2, following Iye et al. 2006). The images of IOK-1 and IOK-2 and their photometric properties are shown in Figure 4 and Table 1, respectively. The color-magnitude diagram ($z' -$ NB973 vs. NB973) of IOK-1 and IOK$-$2, along with all the objects detected down to NB973 $= 24.5$ (total magnitude), is plotted in Figure 5. Their two-color diagram is also shown in Figure 3.

3.4. *Are Objects with Weak NB973 Excess $z = 7$ LAEs?*

As Taniguchi et al. (2005) did in selecting their candidate $z = 6.6$ LAEs, in order not to miss faint targets, we also investigated the possibility that objects with a weak excess of $1.0 > z' -$ NB973 > 3 σ might be $z = 7$ LAEs, even though such objects do not have the expected colors of $z = 7$ LAEs predicted by the stellar population synthesis model outlined in § 3.3 and Figure 3. We define the color criterion of such weak NB973 excess objects as:

3. $B, V, R < 3$ σ, $i' - z' > 1.3$, $1.0 > z' -$ NB973 > 3 σ.

As mentioned in § 3.3, our NB973 is located at the red edge of the z' band. This could cause the criterion (3) to pick up interlopers such as $z = 6.2$–6.8 LAEs/LBGs (as Fig. 3 predicts), $z = 1$–3 extremely red objects (EROs) whose continua have the rest-frame 4000 Å Balmer breaks that result in the NB973 excess vs. z', or M/L/T type red cool dwarf stars whose SEDs can have steep slopes at around the NB973 bandpass. Such objects should be distinguished from $z = 7$ LAEs if they are detected in NB973

TABLE 1
PHOTOMETRIC PROPERTIES OF CANDIDATE Lyα EMITTERS AND NB973-EXCESS OBJECTS

Object	R.A. (J2000.0)	Decl. (J2000.0)	i'	NB816	z'	NB921	NB973	NB973 (total)	Criterion
IOK-1[a]	13 23 59.8	+27 24 55.8	>27.84	>27.04	>27.04	>26.96	24.60	24.40	1
IOK-2	13 25 32.9	+27 31 44.7	>27.84	>27.04	>27.04	>26.96	25.51	24.74	1
IOK-3[b]	13 24 10.8	+27 19 28.1	>27.84	>27.04	26.26	25.08	24.87	24.57	...[c]
Obj-4[d]	13 25 09.1	+27 19 28.1	27.14	26.77	25.75	25.51	24.97	24.85	3
Obj-5[d]	13 23 45.8	+27 32 51.4	>27.84	>27.04	25.76	25.44	25.10	24.74	3

NOTES.—Units of right ascension are hours, minutes, and seconds, and units of declination are degrees, arcminutes, and arcseconds. The values for i', NB816, z', NB921, and NB973 are all 2″ aperture magnitudes, while NB973(total) is a total magnitude. Magnitudes are replaced by their 2 σ limits if they are fainter than the limits. Color criteria are those used to select out candidate LAEs and classify $z' -$ NB973 excess objects (see § 3.3 and 3.4).

[a] IOK-1 was proven to be a $z = 6.96$ LAE spectroscopically by Iye et al. (2006) .

[b] IOK-3 was found to be a $z = 6.6$ LAE by independent spectroscopy by Kashikawa et al. (2006b).

[c] IOK-3 satisfies color criteria (1) and (2) simultaneously, except for NB921 < 3 σ.

[d] These objects show flux excess of $1 > z' -$ NB973 > 3 σ, but could be either $z = 6.2$–6.4 LAEs, low-z ellipticals, or late-type stars (see § 3.4).

as well as z'. From the photometry alone, it is difficult to tell if criterion (3) objects are EROs or dwarfs. However, it is possible to say whether the objects are galaxies at $z = 7$ or not, which is more important to our study.

According to the predicted colors of model galaxies in Figure 3, the criterion (3) should select out $z = 6.2$–6.8 LAEs/LBGs, not $z = 7$ ones. However, since some of $z = 5.7$ LAEs spectroscopically identified by Shimasaku et al. (2006), although not many, do not satisfy their color-selection criteria computed using SED models, objects satisfying our criterion (3), which reside near the border of criteria (1) and (2), could be $z = 7$ LAEs. We found two objects meeting criterion (3) (hereafter referred as to Obj-4, the brighter of the two in 2″ aperture NB973 mag, and Obj-5). Their colors, images, and photometric properties are shown in Figures 3, 4, and 5, and listed in Table 1.

If they are LAEs, their redshifts can be further constrained by using NB816 and NB921 images. As seen in Figure 4, Obj-4 is detected in i', NB816, z', and NB921, as well as NB973, but does not show any significant excess in NB816 vs. i' or in NB921 vs. z', although it displays NB973 excess greater than 3 σ vs. z'. Therefore, it is neither a $z = 5.65$–5.75 LAE nor a $z = 6.5$–6.6 one. Since it is clearly detected in NB816, which is a wave band well shortward of $z = 6.7$–7 Lyα emission, Obj-4 could be a $z = 6.2$–6.4 LAE or LBG.

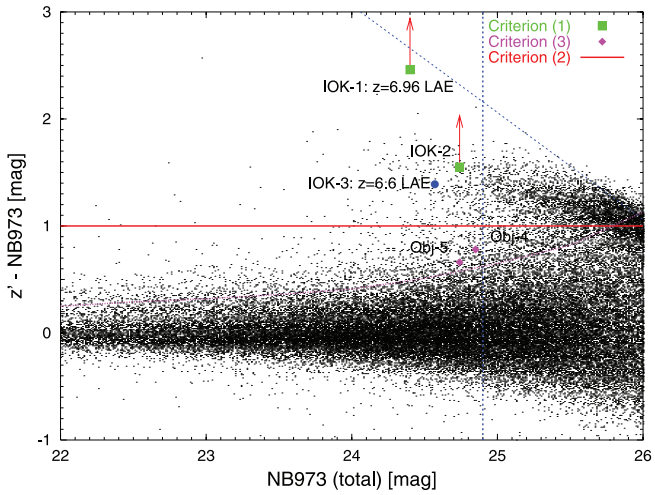

FIG. 5.—$z' -$ NB973 (2″ aperture magnitudes) color as a function of NB973 (total) magnitude of the objects detected in the SDF (*dots*). The dotted curve shows 3 σ error track of $z' -$ NB973 color. The horizontal solid line is a part of our color selection criterion (2), $z' -$ NB973 > 1.0. The vertical dashed line indicates the detection limiting magnitude of our survey, NB973 $= 24.9$ (5 σ). The diagonal dashed line is the 2 σ limit of i' and z' 2″ aperture magnitudes. The IOK-1, 2, and 3, as well as Obj-4 and Obj-5, are shown by the same symbols as in Fig. 3.

On the other hand, Obj-5 is detected in z' and NB921 as well as NB973, but does not show significant excess in NB921 with respect to z', and thus is not a $z = 6.5$–6.6 LAE. Also, detection in NB921 rules out the possibility of $z = 6.7$–7 LAEs, since their fluxes shortward of Lyα should be close to zero. Although it displays an excess of $z' -$ NB973 $> 3\sigma$, its $i' - z'$ color is very similar to that of a $z \sim 5.7$ LAE, which is predicted not to produce any NB973 excess. However, it is not detected in the NB816 image, and thus is not a $z \sim 5.7$ LAE. Hence, Obj-5 could be a LAE or LBG at $z = 6.2$–6.4.

As mentioned earlier, Obj-4 and Obj-5 could be EROs or dwarfs. However, we have confirmed that none of the objects with weak (>3 σ) NB973 excesses (i.e., Obj-4 and Obj-5) can be $z = 7$ LAEs, and thus we do not need to be concerned about the possibility of missing any faint $z = 7$ LAE candidates.

3.5. *Are IOK-1 and IOK-2 Variable Objects?*

As the selection criterion (1) derived in § 3.3 shows, the most probable $z = 7$ LAE candidates are imaged in only the NB973 wave band, and are not detected in any other filters. Since the NB973 image was taken 1–2 yr after the *BVRi'z'* images of the SDF, sources only bright in NB973 could be variable objects such as supernovae or active galactic nuclei (AGNs), which increased their luminosities during our NB973 imaging observation. Therefore, we investigate how many of these objects are likely to be variables. This corresponds to the number of objects that were fainter than our detection limit NB973 $= 24.9$ (5 σ) at some epoch, but become brighter than it at another epoch. Since there are not enough data in the z' and NB973 bands for statistical analysis, we instead used i' band images taken over several separate epochs (T. Morokuma et al. 2008, in preparation) for the best possible (but still somewhat rough) estimation.

First, we calculated the mean color of $i' -$ NB973 over the range of NB973 = 22–25, which is $\langle i' -$ NB973$\rangle = 0.33$, for the purpose of rough conversion of NB973 into i' magnitude. Using this metric, NB973 $= 24.9$ corresponds to $i' = 0.33 + 24.9 = 25.23$. Since the detection limit of the SDF i' band image ($i' = 26.85$ at 5 σ) is firmly deeper, the number count of objects fainter than our NB973 detection limit corresponding to $i' = 25.23$ can be securely obtained down to $i' = 26.85$. The number count per 0.5 mag bin, as well as the magnitude increments needed to exceed NB973 $= 24.9$ in brightness to be detected in NB973, are shown in Table 2. Since we were extrapolating the object number counts in NB973 down to NB973 $= 26.5$ using i' band object number counts down to $i' = 26.85$ (5 σ) and $\langle i' -$ NB973$\rangle = 0.33$, we

TABLE 2
NUMBER COUNTS OF i'-DETECTED OBJECTS FAINTER THAN OUR DETECTION LIMIT NB973 = 24.9

i'[a]	NB973[a]	Δm[b]	$N(i') = N(\Delta m)$[c]
25.23.....	24.9 (5 σ)	0.0	...
25.23–25.33	24.9–25.0	0.0–0.1	2297
25.33–25.83.....	25.0–25.5	0.1–0.6	13589
25.83–26.33.....	25.5–26.0	0.6–1.1	16012
26.33–26.83.....	26.0–26.5	1.1–1.6	17367

NOTE.—Units of the first to third columns are all AB magnitudes with 2″ aperture.
[a] i' band magnitudes were converted into NB973, using $\langle i' - \mathrm{NB973}\rangle = 0.33$.
[b] The NB973 magnitude increments required for objects to become brighter than our detection limit NB973 (5σ) = 24.9. That is, Δm = NB973 − 24.9 or $\Delta m = i' - 25.23$.
[c] The number counts of i'-detected objects.

TABLE 3
NUMBER COUNTS OF OBJECTS IN THE NB973 AND i' IMAGES OF THE SDF

NB973 = $i' - 0.33$[a]	i'[b]	N(NB973)[c]	$N(i')$[d]
22.5–23.0.....	22.83–23.33	2599	2588
23.0–23.5.....	23.33–23.83	3808	3953
23.5–24.0.....	23.83–24.33	5230	5697
24.0–24.5.....	24.33–24.83	7093	8121
24.5–25.0.....	24.83–25.33	8800	10660
25.0–25.5.....	25.33–25.83	...	13589
25.5–26.0.....	25.83–26.33	...	16012
26.0–26.5.....	26.33–26.83	...	17367

NOTE.—Units of the first and second columns are total magnitudes.
[a] i' band magnitudes in the second column were converted into NB973 mag in the first column, using $\langle i' - \mathrm{NB973}\rangle = 0.33$.
[b] i' magnitudes brighter than the 5 σ limiting magnitude of the SDF i' band image $i'(5\ \sigma) = 26.85$.
[c] Number counts of objects detected in the SDF NB973 image down to our detection limit NB973 (5 σ) = 24.9.
[d] Number counts of objects detected in the SDF i' image down to its limiting magnitude $i'(5\ \sigma) = 26.85$.

also checked how similar the number counts in NB973 and in $i' - 0.33$ are to each other, as shown in Figure 6 and Table 3. Since $i' - 0.33$ number counts are slightly larger (by a factor of 1.1–1.2 per bin), our calculation of the number of variables can be only slightly overestimated. Note that the detection completeness of i' and NB973 is not corrected in their number counts, which could be the cause of the smaller counts in NB973 than i' toward our detection limit NB973 = 24.9.

We use in our calculation four i' images of a part of SDF (∼71% of the total area) taken at four separate epochs: 2005 March 4, 2003 April 30, 2002 April 11, and 2001 April 24 (T. Morokuma et al. 2008, in preparation). The number of variable objects $N_v(\Delta i')$ that increased their i' magnitudes by $\Delta i'$ over the periods 2003–2005 and 2001–2002 were counted in each magnitude $\Delta i'$ bin (matched to the Δm bin in Table 2), as shown in Table 4. In the 2003 and 2005 images, ∼70,000 and 80,000 objects were detected down to their limiting magnitudes $i' = 26.3$ and 26.6 (5 σ, 2″ aperture), respectively. Similarly, in the 2001 and 2002 images, ∼50,000 and 70,000 objects were detected down to $i' = 25.9$ and 26.2 (also 5 σ, 2″ aperture),

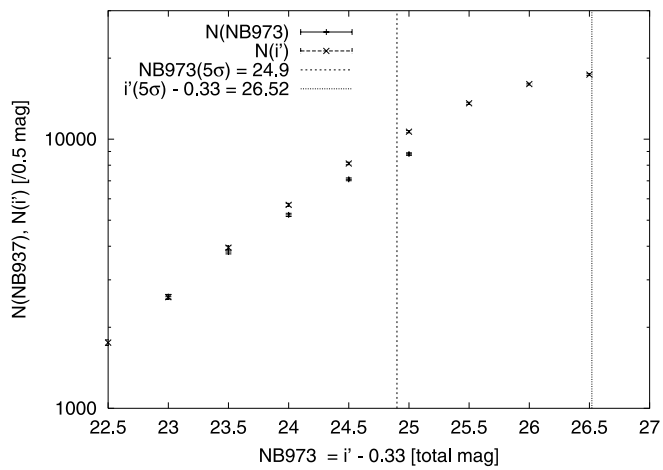

FIG. 6.—Comparison of the number counts of objects detected in the NB973 (*plus symbols*) and i' band (*crosses*) images of SDF down to their detection limits, NB973 = 24.9 (5 σ; *dashed line*) and $i' = 26.85$ (5 σ; *dotted line*), respectively. We try to extrapolate the NB973 number count of objects between NB973 = 24.9 and 26.52 by using the mean color relation of $\langle i' - \mathrm{NB973}\rangle = 0.33$ and the i' band number count at the corresponding magnitude range. Some fraction of such objects could be candidate variables that would become brighter than NB973 = 24.9 at another occasion. Since the i'-band number count is slightly (1.1–1.2 times) higher than that of NB973 at NB973 ≤ 24.9, our extrapolation may be an overestimation.

respectively. Thus, taking the averages, we roughly assumed that $N_{\mathrm{obs}} = 75{,}000$ and 60,000 objects were detected in 2003–2005 and 2001–2002, respectively, and divided the number of variables $N_v(\Delta i')$ by these numbers N_{obj} to obtain the probabilities $P(\Delta i')$ of finding the variables with a brightness increase of $\Delta m = \Delta i'$ in the SDF down to our detection limit.

Finally, multiplying the probability by the number counts of i'-detected objects $N(\Delta m)$ in Table 2 and summing all them up, the number of variables that became brighter than NB973 = 24.9 is ∼9–10. Note that since the magnitude increase of $0 < \Delta m \leq 0.1$ is a small change and cannot be distinguished from photometric errors in NB973 and i' magnitude measurements, which are also of order up to ∼0.1, we ignored the number of variables in the $\Delta m = 0$–0.1 bin at the time of the summation. So far, we have considered only the data for the variables that increased their magnitudes over the two epochs, and did not treat those that decreased their magnitudes. If we roughly assume that their numbers are approximately the same, the number of possible variables could be about one-half of that we estimated above, which is ∼4.5–5. Again, this number might be a slight overestimation by a factor of 1.1–1.2, since for our extrapolation we used the i' band number count instead of that from NB973, which is smaller, as seen in Figure 6 and Table 3. Correcting for this factor, we estimate that the number of variables would be ∼3.8–4.5. This number is slightly different from that reported in Iye et al. (2006), since more elaborate calculations were used here. The estimated number of variables indicates that we cannot completely reject the possibility that the narrowband excess of IOK-1 and IOK-2 is due to object variability. To securely reveal their identities, follow-up spectroscopy is required.

4. SPECTROSCOPY

To confirm the reality of our candidate LAEs, IOK-1 and IOK-2, selected by the color-selection criteria in § 3.3, we carried out optical spectroscopy during 2005–2006 using FOCAS (Kashikawa et al. 2002) on Subaru. The observation status is summarized in Table 5. An Echelle grism (175 lines mm^{-1}, resolution ≃1600) with the z' filter and 0.8″ slit was used to obtain spectra of these objects, in 30 minute exposures each, dithered along the slit by ±1″. The spectrum of a spectrophotometric standard, either Feige 34, Feige 110, or BD +28 4211 (Oke 1990; Hamuy et al. 1994), was also obtained for each night

TABLE 4
NUMBER COUNTS OF i'-DETECTED VARIABLES VS. i' BRIGHTNESS INCREMENT

$\Delta i'$[a] (AB mag)	NUMBER OF VARIABLES, $N_v(\Delta i')$		$P(\Delta i') = N_v(\Delta i')/N_{obj}$[b]		$P(\Delta i') \times N(\Delta m)$	
	2003–2005	2001–2002	2003–2005	2001–2002	2003–2005	2001–2002
0.0	...	...	...	...	...	...
0.0–0.1	250	409	3.3×10^{-3}	6.8×10^{-3}	7.6[c]	15.6[c]
0.1–0.6	52	37	6.9×10^{-4}	6.2×10^{-4}	9.4	8.4
0.6–1.1	1	2	1.3×10^{-5}	3.3×10^{-5}	0.21	0.53
1.1–1.6	1	1	1.3×10^{-5}	1.7×10^{-5}	0.23	0.30
No. variables that became brighter than NB973 = 24.9					9.8[d]	9.2[d]

NOTE.—The number of variables brighter than our detection limit in the stacked i' SDF image, $i' = 0.33 + \mathrm{NB973}(5\ \sigma) = 25.23$, were counted.
[a] Increase in i' magnitude over the two epochs, which is binned to match the third column (Δm) of Table 3.
[b] Probability of finding a variable with a brightness increase of $\Delta i' = \Delta m$ in SDF down to our detection limit.
[c] We ignore these values, since the $\Delta m = 0-0.1$ cannot be distinguished from photometric errors.
[d] These figures were obtained by $\Sigma_{\Delta m} P(\Delta i') \times N(\Delta m) = \Sigma_{\Delta i} P(\Delta i') \times N(\Delta m)$.

and used for flux calibration. The observation data reduction and analysis were all performed in the same manners as in Iye et al. (2006).

4.1. *IOK-1, $z = 6.96$ Lyα Emitter*

We identified IOK-1, the brighter of the two $z = 7$ LAE candidates, as a $z = 6.96$ LAE. The details of the spectroscopic analysis of this object were reported in Iye et al. (2006). We measured the skewness and weighted skewness of the Lyα emission line in the IOK-1 spectrum and obtained $S = 0.558 \pm 0.023$ and $S_w = 9.46 \pm 0.39$ Å, respectively (see Shimasaku et al. [2006] and Kashikawa et al. [2006b] for the definition of S and S_w). These values show that the line is quite asymmetric and ensure that it is a Lyα emission. In fact, our S_w value for IOK-1 is comparable to the average weighted skewness of $z = 5.7$ and 6.6 LAEs (calculated from the data in Shimasaku et al. [2006] and Kashikawa et al. [2006b]), $\langle S_w^{z=5.7} \rangle = 7.43 \pm 1.47$ Å and $\langle S_w^{z=6.6} \rangle = 7.31 \pm 1.51$ Å, respectively.

The Lyα line flux, $F(\mathrm{Ly}\alpha)$, Lyα line luminosity, $L(\mathrm{Ly}\alpha)$, the corresponding star formation rate, SFR(Lyα), and other spectroscopic properties of the Lyα emission line of IOK-1 are summarized in Table 6. To estimate the SFR(Lyα), we use the following relation derived from Kennicutt's equation (Kennicutt 1998) with the case B recombination theory (Brocklehurst 1971):

$$\mathrm{SFR}(\mathrm{Ly}\alpha) = 9.1 \times 10^{-43} L(\mathrm{Ly}\alpha)\ M_\odot\ \mathrm{yr}^{-1}. \quad (1)$$

In addition, we estimate the UV continuum flux, F(UV), by simply subtracting the Lyα emission line flux, $F(\mathrm{Ly}\alpha)$, measured in the spectrum from the NB973 total flux, F_{NB973}, obtained by SExtractor photometry (`MAG_AUTO`),

$$F(\mathrm{UV}) = F_{\mathrm{NB973}} - F(\mathrm{Ly}\alpha). \quad (2)$$

Then, this UV continuum flux can be converted into the UV continuum luminosity, L_ν(UV), and corresponding star formation rate, SFR(UV). To estimate SFR(UV), we use the relation (Kennicutt 1998; Madau et al. 1998)

$$\mathrm{SFR}(\mathrm{UV}) = 1.4 \times 10^{-28} L_\nu(\mathrm{UV})\ M_\odot\ \mathrm{yr}^{-1}. \quad (3)$$

The spectroscopic properties of the UV continuum of IOK-1 are listed in Table 7.

TABLE 5
STATUS OF FOLLOW-UP SPECTROSCOPY

Object	Date (*HST*)	Seeing (arcsec)	Exposure[a] (s)	FOCAS Mask
IOK-1[b]	2005 May 14, 15	0.5–0.7, 0.9–1.0	10800	MOS-1
	2005 Jun 1	0.6–0.8	3600	
	2006 Apr 24	0.9–1.5	16200	
IOK-2[c]	2005 May 14, 15	0.5–0.7, 0.9–1.0	3600	MOS-4
	2006 Apr 24	0.9–1.1	7200	
	2006 Jun 19, 21	1.0–2.0, 1.0–2.0	28430[d]	
	2007 Apr 10	0.4–1.0	28800	
IOK-3	2005 May 14, 15	0.5–0.7, 0.9–1.0	3600	MOS-2
	2005 Jun 1	0.6–0.8	5400	
Obj-4[e]	2005 May 14, 15	0.5–0.7, 0.9–1.0	1800	MOS-5
Obj-5[e]	2005 May 14, 15	0.5–0.7, 0.9–1.0	3600	MOS-3

[a] All the spectra taken during the observation.
[b] Out of all the spectra taken, 11 30 minute exposures were used to obtain the final combined spectrum.
[c] Out of all the spectra taken, 22 30 minute exposures were used to obtain the final combined spectrum.
[d] We did not use data taken at this night because of their low quality (bad seeing).
[e] Not identified yet. Data analyses are in progress.

4.2. *IOK-2*

As reported in Iye et al. (2006) although there appears to be an extremely weak emission-like flux at around 9750 Å ($z = 7.02$ if this is a Lyα line) within the small gap between OH sky lines, 3 hr integration on the IOK-2 spectroscopy (obtained from 2005 May 4 and 2006 April 24) was not deep enough to confirm whether it is real or spurious, since we had only S/N $\sim$ 2 even

TABLE 6
SPECTROSCOPIC PROPERTIES OF THE Lyα EMISSION OF THE $z = 6.96$ LAE

Parameter	Value
Object	IOK-1
z	6.96
$F(\mathrm{Ly}\alpha)$	2×10^{-17} erg s^{-1} cm^{-2}
$L(\mathrm{Ly}\alpha)$	1.13×10^{43} erg s^{-1}
SFR(Lyα)	10.24 $M_\odot$ yr^{-1}
FWHM	13 Å, 403 km s^{-1}
S_w	9.46 ± 0.39 Å
S/N	5.5

TABLE 7
SPECTROSCOPIC PROPERTIES OF THE UV CONTINUUM OF THE $z = 6.96$ LAE

Parameter	Value
Object	IOK-1
z	6.96
L_ν(UV)	2.58×10^{29} erg s^{-1} Hz^{-1}
SFR(UV)	36.1 $M_\odot$ yr^{-1}

though measured within the gap. This did not allow us to draw any firm conclusions about IOK-2.

To reveal the true entity of this object, we made additional 8 hr follow-up spectroscopy with Subaru/FOCAS on 2007 April 10 (see Table 5). The seeing during this observing run was 0.4″–1″ with clear sky. We combined the spectra taken at this night with those obtained in 2006 and 2005 to achieve the total of 11 hr integration. However, the sky-subtracted stacked spectrum shows neither the emission-like flux at 9750 Å nor any other spectral features. We also combined only the spectra taken in 2007 and again could not find any emission lines. There are no signals that follow the dithering shifts among 30 minute spectrum frames. This result indicates that the extremely weak emission-like flux at 9750 Å seen in 3 hr stacked spectrum made from 2005 and 2006 frames is spurious.

To see whether our 11 hr spectroscopy has reached the depth required to detect a Lyα emission, we compare the sky background rms of the stacked spectrum with the Lyα flux calculated from the NB973 magnitude of IOK-2. If we assume that all of the flux in NB973 comes from the Lyα line at $z = 7$ and adopt the total magnitude of NB973 = 24.74 rather than the 2″ aperture one, we obtain a line flux of $F^{\rm phot}({\rm Ly}\alpha) = 2.9 \times 10^{-17}$ erg s^{-1} cm^{-2}. On the other hand, binning of 4 pixels (corresponding to 0.017 Mpc at $z = 7$) in the spatial direction is used to extract the one-dimensional spectrum. The sky rms (in terms of flux density) is measured in this spectrum by calculating the variance in unbinned pixels along the dispersion direction within the wavelength range corresponding to NB973 passband 9655–9855 Å, and it is found to be 3.0×10^{-19} erg s^{-1} cm^{-2} Å^{-1}. The FWHM of the Lyα line, for example, of a $z = 6.6$ LAE varies from 5.5 to 14.6 Å (Kashikawa et al. 2006b; Taniguchi et al. 2005). If we assume that the FWHM distribution of $z = 7$ LAEs is similar, then we obtain a Lyα line flux of $F^{\rm spec}({\rm Ly}\alpha) = (1.7\text{–}4.4) \times 10^{-18}$ erg s^{-1} cm^{-2}. This is 6.6–17 times fainter than $F^{\rm phot}({\rm Ly}\alpha)$, indicating that we have reached a sufficient depth to detect the Lyα line if IOK-2 is a real LAE at $z = 7$. Likewise, even if we use the 2″ aperture magnitude of NB973 = 25.51, we obtain $F^{\rm phot}({\rm Ly}\alpha) = 1.4 \times 10^{-17}$ erg s^{-1} cm^{-2}, and $F^{\rm spec}({\rm Ly}\alpha)$ is 3.2–8.2 times fainter than this. Furthermore, even if we assume that only ∼68% of the NB973 flux comes from Lyα line, as Iye et al. (2006) did, $F^{\rm spec}({\rm Ly}\alpha)$ is still 4.5–12 (2.2–5.6) times fainter than $F^{\rm phot}({\rm Ly}\alpha)$ if we use the NB973 total (2″ aperture) magnitude to calculate $F^{\rm phot}({\rm Ly}\alpha)$. In all cases we have considered, our spectroscopy reached sufficient depth to detect a Lyα line. Hence, IOK-2 might not be a LAE. However, we should note that residuals of the subtracted OH sky lines around 9790 Å in the 11 hr stacked spectrum are still locally strong (∼13% of the NB973 passband is contaminated), and a Lyα line could be masked out if it is weak and redshifted there.

If IOK-2 is not a LAE, the possible origin of the NB973 flux excess could be either a LBG at $z \sim 7$, a low-z ERO, a late-type star, a variable object, or noise. In the first three cases, spectroscopy would show no signals in the spectrum if their continuum light is very faint. If IOK-2 is a variable object, a distinct possibility, as discussed in § 3.5, it could be fainter than our detection limit at the time of the follow-up spectroscopy. The possibility that IOK-2 is a noise spike in the NB973 image also cannot be ruled out, although it is very low, as described in Iye et al. (2006). An additional NB973 imaging of SDF will be helpful to see whether IOK-2 is either a variable object or noise. For the statistical analysis in the following sections, we assume that only IOK-1 is a $z = 7$ LAE we have successfully identified, and IOK-2 is not.

5. IMPLICATIONS FOR REIONIZATION AND GALAXY EVOLUTION

From $z \sim 6$ quasar GP diagnostics, the neutral IGM fraction at this redshift is estimated to be $x_{\rm H\,I}^{z\sim6.2} \sim 0.01\text{–}0.04$, and thus the reionization is believed to have already completed at around this epoch (Fan et al. 2006). This result is also supported by the spectral modeling analysis of the currently most distant GRB at $z \sim 6.3$ conducted by Totani et al. (2006), placing the constraint of $0 \le x_{\rm H\,I}^{z\sim6.3} < 0.17\text{–}0.6$.

On the other hand, the observed Lyα LFs of LAEs at $z \sim 6$ and higher redshifts can be used to probe the epoch of reionization. The Lyα LF is expected to decline beyond $z \sim 6$ due to a rapid change of neutral IGM and ionization states before and after the completion of reionization (Haiman & Spaans 1999; Rhoads & Malhotra 2001; Hu et al. 2002). While the Lyα LF has been observed not to evolve at $z = 3\text{–}5.7$ (Ouchi et al. 2003; Ajiki et al. 2003; Tran et al. 2004; van Breukelen et al. 2005), it was recently found to decline as $L^*_{z=6.6} \sim (0.4\text{–}0.6)L^*_{z=5.7}$ from $z = 5.7$ to 6.6 in the SDF, suggesting that $x_{\rm H\,I}^{z=6.6} \le 0.45$ (Kashikawa et al. 2006b). Furthermore, we also found that the number density of $z = 7$ LAEs is only 18%–36% of the density at $z = 6.6$ (Iye et al. 2006). This series of decrements in densities might reflect the completion of reionization at around $z \sim 6$, beyond which the fraction of the neutral IGM hydrogen could possibly increase and attenuate the Lyα photons from LAEs.

However, this interpretation was based on the assumption that there was no evolution of the LAE population from $z = 5.7$ to 7. The recent photometric study of $z \sim 6$ *i*-dropouts and $z \sim 7\text{–}8$ *z*-dropouts in the Hubble Ultra Deep Field (UDF) demonstrated that the galaxy number density decreases by a factor of ∼0.1–0.2, suggesting the rapid evolution of luminous galaxies between these epochs (Bouwens & Illingworth 2006).

In the following discussion, we re-evaluate the comparison of our LAE number and Lyα luminosity densities at $z = 7$ with those at $z = 5.7$ and 6.6, using the most up-to-date SDF data from Shimasaku et al. (2006) and Kashikawa et al. (2006b). We also investigate the possibility of LAE galaxy evolution between $z = 5.7$ and 7 and the degree to which it might contribute to the number density deficit between these epochs.

5.1. *The Evolution of the Lyα LF at $z \gtrsim 6$*

Figure 7 compares Lyα line LFs at $z = 5.7$, 6.6, and 7 derived from the latest SDF data (i.e., Shimasaku et al. 2006; Kashikawa et al. 2006b; Iye et al. 2006). In addition, Figure 8 shows the LAE number densities, $n_{\rm Ly\alpha}$, Lyα line luminosity densities, $\rho_{\rm Ly\alpha}$, and corresponding star formation rate densities, SFRD$_{\rm Ly\alpha}$, at $2.3 < z \le 7$ down to our detection limit $L_{\rm limit}({\rm Ly}\alpha) = 1.0 \times 10^{43}$ erg s^{-1} (converted from NB973 ≤ 24.9 [5 σ], as Iye et al. [2006] did). The $\rho_{\rm Ly\alpha}$ and SFRD$_{\rm Ly\alpha}$ at $z = 7$ are calculated using Lyα line luminosity estimated from the spectrum of IOK-1 and equation (1). The number and luminosity densities at $z < 7$ are obtained by integrating the best-fit Lyα Schechter

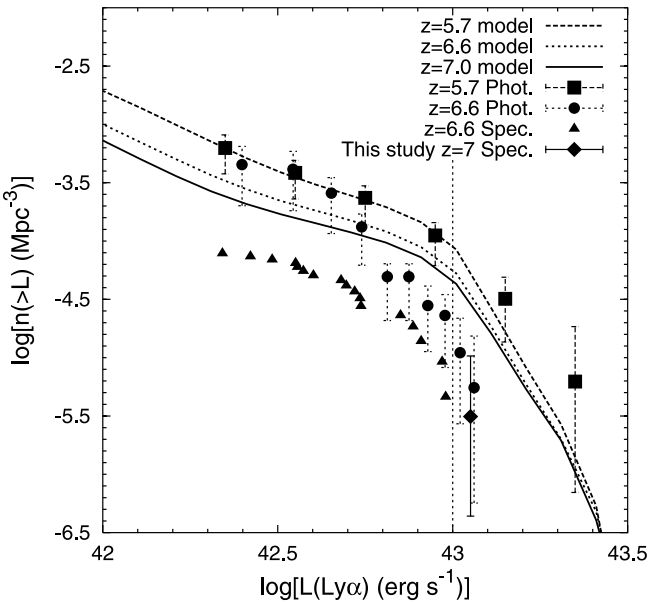

FIG. 7.—Cumulative Lyα LFs of LAEs at $z = 5.7$ (Shimasaku et al. 2006; filled squares for their photometric LF), 6.6 (Kashikawa et al. 2006b; filled circles and triangles for their photometric [upper limit] and spectroscopic [lower limit] LFs, respectively), and 7 (this study; diamond for IOK-1 spectroscopic data). All the errors include cosmic variance and Poissonian errors for small-number statistics (see § 5.1 for details). All the data and errors are corrected for detection completeness. The long-dashed, short-dashed, and solid curves show the intrinsic (i.e., not affected by neutral IGM) Lyα LFs at $z = 5.7$, 6.6, and 7, respectively, predicted by K07 LAE evolution model (see § 5.2.3). The vertical dashed line shows our survey limit down to which the LFs are integrated to obtain LAE number and luminosity densities.

LFs (Schechter 1976) of LAEs down to our detection limit $L_{\rm limit}({\rm Ly}\alpha)$ as

$$\phi(L)dL = \phi^*\left(\frac{L}{L^*}\right)^{\alpha}\exp\left(\frac{-L}{L^*}\right)d\left(\frac{L}{L^*}\right), \quad (4)$$

$$n_{{\rm Ly}\alpha} = \int_{L_{\rm limit}}^{\infty}\phi(L)\,dL, \quad (5)$$

$$\rho_{{\rm Ly}\alpha} = \int_{L_{\rm limit}}^{\infty}\phi(L)L\,dL. \quad (6)$$

We adopt $\{\log(\phi^*[{\rm Mpc}^{-3}]), \log(L^*[{\rm erg\ s}^{-1}]), \alpha\} = \{-3.44^{+0.20}_{-0.16}, 43.04^{+0.12}_{-0.14}, -1.5\}$ and $\{-2.88^{+0.24}_{-0.26}, 42.60^{+0.12}_{-0.10}, -1.5\}$ for Lyα LFs of LAEs at $z = 5.7$ and 6.6 in the SDF (taken from Table 3 in Kashikawa et al. 2006b), respectively. The values $\phi^* = (22.0 \pm 12.0, 1.7 \pm 0.2)\times10^{-4}$ Mpc^{-3} and $L^* = (5.4 \pm 1.7, 10.9 \pm 3.3)\times10^{42}$ erg s^{-1} with $\alpha = -1.6$ are quoted for $2.3 < z < 4.5$ (van Breukelen et al. 2005) and $z \sim 4.5$ (Dawson et al. 2007) Lyα LFs, respectively. We also use $\phi^* = (9.2^{+2.5}_{-2.1}, 3.4^{+1.0}_{-0.9}, 7.7^{+7.4}_{-3.9})\times10^{-4}$ Mpc^{-3} and $L^* = (5.8^{+0.9}_{-0.7}, 10.2^{+1.8}_{-1.5}, 6.8^{+3.0}_{-2.1})\times10^{42}$ erg s^{-1} with $\alpha = -1.5$ for Lyα LFs of LAEs at $z = 3.1$, 3.7, and 5.7 in $\sim$1.0 deg^2 of the SXDS field (Ouchi et al. 2007). The $\rho_{{\rm Ly}\alpha}$ is converted to SFRD$_{{\rm Ly}\alpha}$ using equation (1).

The uncertainties in the number and luminosity densities at $z = 5.7$–7 of LAEs in the SDF in Figure 7 and 8 (and likewise Figs. 9 and 10) include cosmic variance and the Poissonian errors associated with small-number statistic. To estimate the cosmic variance σ_v at $z = 5.7$–7, we adopt a bias parameter $b = 3.4 \pm 1.8$ derived from the sample of 515 $z = 5.7$ LAEs detected in $\sim$1.0 deg^2 of the SXDS field (Sekiguchi et al. 2004; Ouchi et al. 2005), which is $\sim$5 times wider than the SDF. Then, applying the dark matter halo variances $(z, \sigma_{\rm DM}) = (5.7, 0.063), (6.6, 0.053)$ and (7.0, 0.044) obtained using the analytic cold dark matter model (Sheth & Tormen 1999; Somerville et al. 2004) and our SDF survey volumes to $b = \sigma_v/\sigma_{\rm DM}$, we calculate the geometric mean of cosmic variance at $z = 5.7$–7, which is 8.4%–27%. The maximum cosmic variance of $\sigma_v = 27\%$ is included in the errors in Figures 7–10. Similarly, the cosmic variance at $z = 2.3$–4.5 is also calculated and included in Figure 8. The Poissonian errors for small-number statistic are estimated using Tables 1 and 2 in Gehrels (1986). When the densities and errors are calculated for $z = 5.7$, 6.6, and 7 LAEs in the SDF, the detection completenesses in NB816, NB921, and NB973 images are also corrected (see Fig. 2 for NB973 completeness).

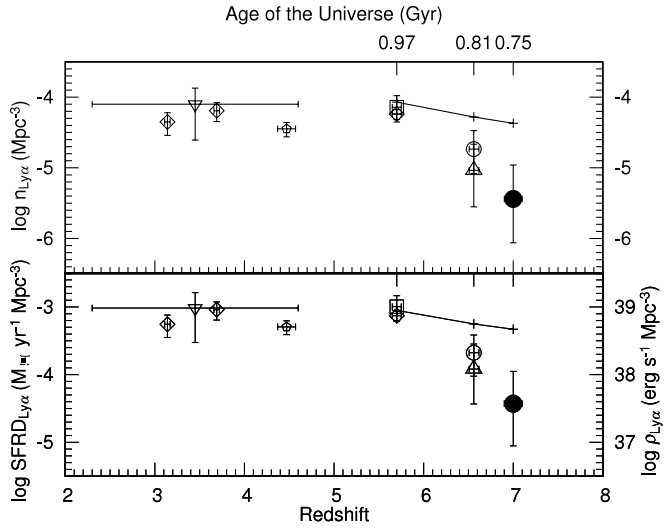

FIG. 8.—Number density $n_{{\rm Ly}\alpha}$, Lyα line luminosity density $\rho_{{\rm Ly}\alpha}$, and star formation rate density SFRD$_{{\rm Ly}\alpha}$ of LAEs at $z = 5.7$, 6.6, and 7 derived from the latest Subaru/Suprime-Cam LAE surveys and those at $2.3 < z < 5.7$ from the literature down to $L_{\rm limit}({\rm Ly}\alpha) = 1.0\times10^{43}$ erg s^{-1}. The densities at $z = 5.7$, 6.6, and 7 in the SDF are calculated from the photometric sample of Shimasaku et al. (2006; *open squares*), the photometric and spectroscopic samples of Kashikawa et al. (2006b; *open circles and triangles, respectively*), and the IOK-1 spectrum (*large filled circles*), respectively. Densities at $2.3 < z < 4.5$ and $z \sim 4.5$ are calculated using the best-fit Lyα Schechter LFs from van Breukelen et al. (2005; *inverse triangle*) and Dawson et al. (2007; *pentagon*), respectively. Also, densities at $z = 3.1$, 3.7, and 5.7 in the $\sim$1.0 deg^2 of SXDS field are calculated using the best-fit Lyα Schechter LFs from Ouchi et al. (2007; *diamonds*). Each horizontal error bar shows the redshift range of each survey. The vertical error bars at $z = 5.7$, 6.6, and 7 include both cosmic variance and Poissonian errors for small-number statistics, while those at $z < 5.7$ contain only cosmic variance, since Poissonian errors for them are negligibly small (see § 5.1 for details). The data and vertical error bars at $z = 5.7$, 6.6, and 7 are corrected for their detection completeness. The plus symbols at $z = 5.7$, 6.6, and 7 with solid lines show the expected densities obtained by integrating the intrinsic (i.e., not affected by neutral IGM) Lyα LFs predicted by the K07 LAE evolution model in § 5.2.3. At $z > 5.7$, the densities clearly decrease with increasing redshifts and are smaller than the model-predicted values, implying that the Lyα lines might be attenuated by the possibly increasing neutral IGM at the reionization epoch.

While it remains unchanged at $2.3 < z < 5.7$, the LAE number density decreases by a factor of $n_{{\rm Ly}\alpha}^{z=6.6}/n_{{\rm Ly}\alpha}^{z=5.7} \simeq 0.24$ from $z = 5.7$ to 6.6 and $n_{{\rm Ly}\alpha}^{z=7}/n_{{\rm Ly}\alpha}^{z=6.6} \simeq 0.17$ from $z = 6.6$ to 7. Similarly, the LAE Lyα luminosity density declines by factors of $\rho_{{\rm Ly}\alpha}^{z=6.6}/\rho_{{\rm Ly}\alpha}^{z=5.7} \simeq 0.21$ and $\rho_{{\rm Ly}\alpha}^{z=7}/\rho_{{\rm Ly}\alpha}^{z=6.6} \simeq 0.15$. If we assume that the LAE population does not evolve from $z = 7$ to 5.7, this density deficit might reflect an increase in neutral IGM hydrogen with redshifts.

However, the density decline might also possibly be ascribed to the evolution of the LAE population. If the number of LAEs having luminosities fainter than our SDF detection limits drastically

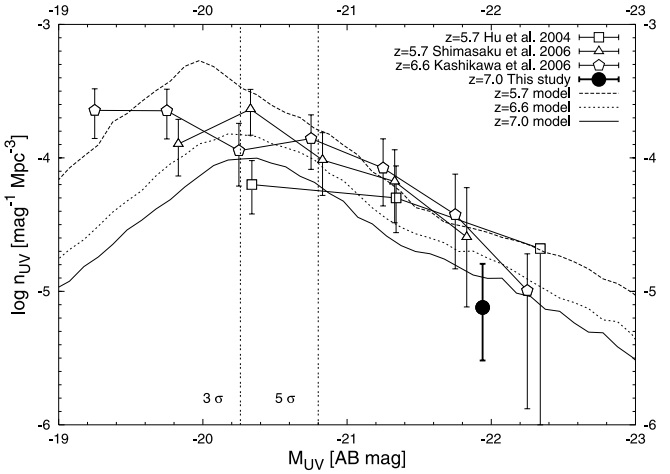

FIG. 9.—Rest-frame UVLFs (per unit absolute magnitude) of $z = 5.7$ and 6.6 LAEs compared with that at $z = 7$ derived using IOK-1 data. Our survey detection limits at 5 σ and 3 σ are shown by vertical dashed lines. The errors include cosmic variance and Poissonian errors for small-number statistics (see § 5.1 for details). All the data and errors are corrected for their detection completeness. The $z = 7$ UVLF does not evolve from $z = 5.7$ to 6.6. The long-dashed, short-dashed, and solid curves show UVLFs of LAEs at $z = 5.7$, 6.6, and 7 predicted by the K07 model, respectively. They are in good agreement with observed data.

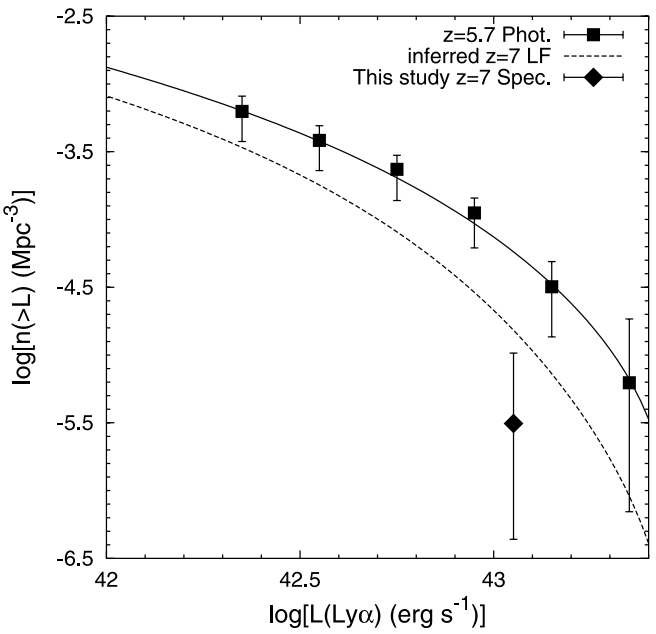

FIG. 10.—Cumulative Lyα LFs of LAEs at $z = 5.7$ (Shimasaku et al. 2006; *filled squares*) and 7 (this study; *diamond*). Errors include cosmic variance and Poissonian errors for small-number statistics (see § 5.1 for details). All the data and errors are corrected for detection completeness. The solid curve is the best-fit $z = 5.7$ Schechter LF (see § 5.1). The dashed curve is the same Lyα Schechter LF, but made to evolve from $z = 5.7$ to 7 by imposing $L^{*,\mathrm{expect}}_{z=7} \sim 0.58 L^{*}_{z=5.7}$ obtained using the correlation of $\Delta M^{*}_{\mathrm{UV}}/\Delta z \sim 0.47$ extrapolated from the result of Yoshida et al. (2006; see their Fig. 22), and assuming that the same correlation can also hold for Lyα luminosity (see § 5.2.2).

increases from $z = 5.7$ to 7, this could certainly affect our estimations of $n_{\mathrm{Ly}\alpha}$ and $\rho_{\mathrm{Ly}\alpha}$. Hence, the Lyα LF alone cannot resolve this degeneracy between the reionization and galaxy evolution effects.

To cope with this matter, the rest-frame UV continuum luminosity function (UVLF) of LAEs can be used to extract the galaxy evolution effect alone, since it is not suppressed by neutral hydrogen. Kashikawa et al. (2006b) have compared the UVLF (rest frame $\sim$1255 Å at $z = 6.6$ and $\sim$1350 Å at $z = 5.7$) of LAEs in the SDF and other fields also imaged by Suprime-Cam, and found that it does not significantly change from $z = 5.7$ to 6.6. This suggests that the density deficit between $z = 5.7$ and 6.6 is not mainly caused by galaxy evolution. Thus, Kashikawa et al. (2006b) concluded that reionization might have ended at around $5.7 < z < 6.6$, which supports the results of $z \sim 6$ quasars and GRBs (Fan et al. 2006; Totani et al. 2006). If this is also the case for $z = 6.6$–7 LAEs, the further decline of LAE density implies an increase in neutral hydrogen that attenuates Lyα photons and supports the results of Kashikawa et al. (2006b).

5.2. *Can the Lyα Evolution be Explained Only by Galaxy Evolution?*

We do not know whether the LAEs themselves evolve at $z = 6.6$–7. If galaxy evolution occurs at $z = 6.6$–7, the further decline of LAE density at these epochs reflects it in addition to reionization. Hence, in this section, we investigate the possibilities of LAE evolution from $z = 6.6$ to 7 using three independent methods: (1) comparison of the UVLFs of $z = 5.7$ and 6.6 LAEs with that of $z = 7$ LAEs derived from our spectroscopic data of IOK-1, (2) estimation from the UVLF evolution of LBGs, and (3) application of an LAE evolution model constructed by Kobayashi et al. (2007) based on a hierarchical clustering galaxy formation model (Nagashima & Yoshii 2004) to predict the expected change in the Lyα LF from $z = 7$ to 5.7 due to galaxy evolution alone.

5.2.1. *Implications from UVLF of $z = 7$ LAEs*

First, we roughly estimate the UVLF of $z = 7$ LAEs to see if there is any possible galaxy evolution from $z = 6.6$. We calculate the absolute UV magnitude $M_{\mathrm{UV},1230}$ at rest frame 1230 Å for IOK-1 from the UV continuum flux $F(\mathrm{UV})$ obtained in § 4.1 using equation (2), and $F(\mathrm{Ly}\alpha)$ measured in the spectrum of IOK-1. That is,

$$\begin{aligned} M_{\mathrm{UV},1230} &= m_{\mathrm{UV},1230} - \mathrm{DM} + 2.5\log(1+z) \\ &= -2.5\log\left[\frac{\lambda^2}{c\Delta\lambda}F(\mathrm{UV})\right] \\ &\quad - 48.6 - \mathrm{DM} + 2.5\log(1+z), \end{aligned} \tag{7}$$

where $m_{\mathrm{UV},1230}$ is the UV apparent magnitude, $\lambda = 1230(1+z)$ Å, $\Delta\lambda$ is the wavelength range in which the UV continuum is covered by NB973 passband, $\Delta\lambda = 9855$ Å $- (1+z)1216$ Å, DM is the distance modulus, and c is the speed of light. Figure 9 shows the UVLF of $z = 7$ LAEs derived here together with those of $z = 5.7$ and 6.6 LAEs. We ignore a subtle difference in the rest-frame UV wavelengths (rest frame $\sim$1230 Å at $z = 7.0$, $\sim$1255 Å at $z = 6.6$, and $\sim$1350 Å at $z = 5.7$), assuming that the LAEs have flat UV continua. The detection completeness of the NB973 image is also corrected using Figure 2. The UVLF implies that there is no galaxy evolution from $z = 7$ to 6.6, and the density deficits of $n_{\mathrm{Ly}\alpha}$ and $\rho_{\mathrm{Ly}\alpha}$ between these epochs might be attributed mainly to reionization.

5.2.2. *Estimation from the UVLF Evolution of LBGs*

Even though the $z = 7$ UVLF derived from the SDF data suggests that LAEs do not evolve from $z = 7$ to 6.6, it suffers from small statistics due to the relatively shallower detection limit in NB973 [equivalent to $L(\mathrm{Ly}\alpha) \geq 1.0 \times 10^{34}$ erg s^{-1}]. Therefore, we discuss the possibilities of the LAE galaxy evolution at

$z = 5.7$–7 using inferences from other independent methods, by which we try to obtain some helpful insights.

One possible way to estimate the LAE galaxy evolution at $z = 5.7$–7 is inference from the evolution of the UVLF of high-z LBGs, assuming that LAEs and LBGs share a similar evolutionary history. We use the UVLF data from the recent observational studies of $z \sim 4$–8 LBGs conducted by Yoshida et al. (2006), Bouwens et al. (2006), and Bouwens & Illingworth (2006). Their surveys, when combined together, form the deepest and widest imaging data, with samples having the largest numbers of all LBG surveys. Interestingly, Yoshida et al. (2006) combined their data for $z \sim 4$ and 5 LBGs with those from lower-z LBG surveys and the $z \sim 6$ LBG (i-dropout) study by Bouwens et al. (2006) and found a clear evolution of the UVLF from $z \sim 6$ to 0, in which only the characteristic magnitude, $M^*_{\rm UV}$, changes significantly and almost linearly with redshift, while the normalization factor, ϕ^*, and the faint-end slope, α, tend to remain constant, as seen in Figure 22 of Yoshida et al. (2006). This trend of $M^*_{\rm UV}$, ϕ^*, and α vs. z continues up to $z \sim 7.4$, when we add $M^*_{\rm UV} = -19.5 \pm 0.6$ mag, $\phi^* = 0.00202^{+0.00086}_{-0.00076}$ Mpc^{-3}, and $\alpha = -1.73$ (or $M^*_{\rm UV} = -18.75 \pm 0.6$ mag, $\phi^* = 0.00218$ Mpc^{-3}, and $\alpha = -1.73$) of the first (or second) LBG UVLF at $z \sim 7.4$ derived by Bouwens & Illingworth (2006).

We estimate the change in $M^*_{\rm UV}$ between $z = 5.7$ and $z = 7$ from the z-dependence of $M^*_{\rm UV}$ at $z \sim 4$, 5, 6, and 7.4, assuming that the correlation is linear, with a slope of $\Delta M^*_{\rm UV}/\Delta z \simeq 0.47$ mag. As a result, $M^*_{\rm UV}$ is expected to become fainter by 0.6 mag, which corresponds to a luminosity of $L^{*,{\rm expect}}_{z=7} \simeq 10^{-0.4\times0.6} L^*_{z=5.7} \simeq 0.58 L^*_{z=5.7}$. Here, the relation between the equation (4) and the Schechter LF in absolute magnitude form,

$$\phi(M)dM = \frac{2}{5}\phi^*(\ln 10)\left[10^{(2/5)(M^*-M)}\right]^{\alpha+1} \times \exp\left[-10^{(2/5)(M^*-M)}\right]dM, \quad (8)$$

is used to convert $M^*_{\rm UV}$ to L^*. To infer the deficit by which Lyα LF of LAEs decreases from $z = 5.7$ to 7 due to their evolution alone, we now roughly assume that this UVLF evolution of the LBGs can also be applied to LAEs at $z = 5.7$–7, and that Lyα line luminosities of LAEs are simply proportional to their UV continuum luminosities, as Figure 15 in Taniguchi et al. (2005) suggests. Based on this idea, we change $L^*_{z=5.7}$ of our best-fit Schechter Lyα LF at $z = 5.7$ in exactly the same way (i.e., $\log(\phi^*[{\rm Mpc}^{-3}]) = -3.44^{+0.20}_{-0.16}$ and $\alpha = -1.5$ as in § 5.1 but $\log(L^*_{z=5.7}[{\rm erg\ s^{-1}}]) = 43.04^{+0.12}_{-0.14} + \log 0.58$ here), to obtain the $z = 7$ Lyα LF. This result is compared in Figure 10 with actual observational data of IOK-1.

The inferred Lyα LF at $z = 7$ does not really agree with one calculated from the spectrum of IOK-1. Our density deficit between $z = 5.7$ and 7 LAEs cannot be explained by only the galaxy evolution factor estimated here. The integrations of the inferred Lyα LF using equations (5) and (6) down to $\log L({\rm Ly}\alpha) = 43.05$, which is IOK-1's Ly$\alpha$ line luminosity, yield $n^{{\rm expect},z=7}_{{\rm Ly}\alpha} \simeq 1.5 \times 10^{-5}$ Mpc^{-3} and $\rho^{{\rm expect},z=7}_{{\rm Ly}\alpha} \simeq 2.3 \times 10^{38}$ erg s^{-1} Mpc^{-3}, respectively. Our LAE number and Lyα line luminosity densities at $z = 7$ are $n^{z=7}_{{\rm Ly}\alpha} \simeq (3.6^{+7.3}_{-2.8}) \times 10^{-6}$ Mpc^{-3} and $\rho^{z=7}_{{\rm Ly}\alpha} \simeq (4.1^{+8.2}_{-3.1}) \times 10^{37}$ erg s^{-1} Mpc^{-3} based on IOK-1 data alone, respectively. Therefore, the density deficits of $n^{z=7}_{{\rm Ly}\alpha}/n^{{\rm expect},z=7}_{{\rm Ly}\alpha} \simeq 0.24^{+0.49}_{-0.19}$ and $\rho^{z=7}_{{\rm Ly}\alpha}/\rho^{{\rm expect},z=7}_{{\rm Ly}\alpha} \simeq 0.18^{+0.36}_{-0.13}$ might be due to the attenuation of Lyα photons by neutral IGM existing during reionization.

In order for the inferred Lyα LF at $z = 7$ to have the same number density as the observed Lyα LF at $z = 7$ (i.e., $n^{{\rm expect},z=7}_{{\rm Ly}\alpha} = n^{z=7}_{{\rm Ly}\alpha}$), we have to change the characteristic luminosity $L^{*,{\rm expect}}_{z=7}$ by a factor of $0.65^{+0.24}_{-0.18}$. This factor might reflect the deficit by which the Lyα LF of LAEs decreases from $z = 5.7$ to 7 due to the attenuation of the Lyα lines of LAEs by the increasing neutral IGM during reionization beyond $z \sim 6$. We can refer to such a deficit factor due to neutral IGM attenuation as the IGM transmission to Lyα photons, $T^{\rm IGM}_{{\rm Ly}\alpha}$. In the case of our discussion so far, this can be regarded as the ratio of the Lyα line luminosities of LAEs in the environments with some neutral IGM fraction $x_{\rm H\,I}$ still remaining to those in environments with no neutral IGM (i.e.,, $x_{\rm H\,I} = 0$), $T^{\rm IGM}_{{\rm Ly}\alpha} = L^{x_{\rm H\,I}}({\rm Ly}\alpha)/L^{x_{\rm H\,I}=0}({\rm Ly}\alpha)$. Once we know $T^{\rm IGM}_{{\rm Ly}\alpha}$, the neutral IGM fraction at $z = 7$, $x^{z=7}_{\rm H\,I}$, can be estimated. However, the calculation of $x_{\rm H\,I}$ from $T^{\rm IGM}_{{\rm Ly}\alpha}$ is not a simple issue and is dependent on theoretical models. We will discuss it in § 5.3.

Similarly, the z-dependence of $M^*_{\rm UV}$, $\Delta M^*_{\rm UV}/\Delta z \simeq 0.47$ mag, predicts $\Delta M^*_{\rm UV} \simeq 0.42$ for $\Delta z = 6.6$–5.7, and thus $L^{*,{\rm expect}}_{z=6.6} \simeq 10^{-0.4\times0.42} L^*_{z=5.7} \simeq 0.68 L^*_{z=5.7}$ due to LAE galaxy evolution from $z = 6.6$ to 5.7. However, Kashikawa et al. (2006b) found that the Lyα LF declines in such a way that $L^*_{z=6.6} \sim (0.4$–$0.6) L^*_{z=5.7}$ from $z = 5.7$ to 6.6, regarding their photometric and spectroscopic LFs as the upper and lower limits of the $z = 6.6$ Lyα LF, respectively. Hence, the attenuation of Lyα photons by the neutral IGM at $z = 6.6$ is $T^{\rm IGM}_{{\rm Ly}\alpha} = L^*_{z=6.6}/L^{*,{\rm expect}}_{z=6.6} \simeq 0.59$–$0.88$.

The decrease in Lyα LF from $z = 5.7$ to 6.6 and 7 cannot be explained only by the evolution of LAEs, as inferred from that of LBGs. This result implies that the remaining deficits could come from the attenuation of Lyα lines by the neutral IGM. If this is the case, the Lyα line will tend to be more attenuated at higher redshift as $T^{\rm IGM}_{{\rm Ly}\alpha} \simeq 0.59$–$0.88$ at $z = 6.6$ and $0.65^{+0.24}_{-0.18}$ at $z = 7$, implying that the neutral IGM fraction, $x_{\rm H\,I}$ increases with redshift beyond $z \sim 6$, as derived in § 5.3. However, note that this result is based on the assumption that LAEs evolve in the same way as LBGs. This might not be necessarily true. Although the LAEs are believed to be closely related to LBGs and many of candidate LBGs at high redshift have been identified as LAEs by spectroscopy, the link between these two populations has not been clearly understood yet, and they might have followed different evolutionary histories.

5.2.3. *Application of a Galaxy Evolution Model*

In the previous sections, we tried to estimate the intrinsic evolution of the Lyα LF of LAEs from the UVLF evolution of LAEs and LBGs, with an implicit assumption that the evolutions of Lyα and UV luminosities are similar. However, this assumption may not be true in reality, and hence our argument will be strengthened if we can show that these are indeed similar in a realistic theoretical model of LAEs.

For this purpose, we use a recent model for LAE evolution constructed by Kobayashi et al. (2007, hereafter K07). This model is an extension of one of the latest hierarchical clustering models of galaxy formation (Nagashima & Yoshii 2004), in which the merger histories of dark matter halos are modeled based on structure formation theory, and star formation processes in dark halos are calculated to predict the photometric properties of galaxies. This model can reproduce most of the observed photometric, kinematic, structural, and chemical properties of local galaxies, as well as high-z LBGs (Kashikawa et al. 2006a). K07 extended this model without changing the original model parameters, but introducing new modeling for the escape fraction of Lyα photons ($f^{{\rm Ly}\alpha}_{\rm esc}$) from galaxies based on physical considerations. Specifically, the dust extinction of Lyα photons and the effect of galaxy-scale outflow are newly taken into account. This is the first model for LAEs based on a hierarchical galaxy

TABLE 8
NEUTRAL IGM FRACTIONS OBTAINED BY SEVERAL INDEPENDENT METHODS

METHOD	NEUTRAL FRACTIONS $x_{\rm H\,I}$			
	$z\sim6$	$z\sim6.3$	$z=6.6$	$z=7.0$
1. Quasar GP test	0.01–0.04	...	...	...
2. GRB	...	<0.17–0.60	...	...
3. Lyα LF	...	...	<0.45	...
4. Lyα LF and LBG UVLF	...	...	~0.12–0.42	~0.12–0.54
5. Model and observed Lyα LFs	...	...	~0.24–0.36	~0.32–0.64

NOTES.—Method sources: (1) Fan et al. 2006; (2) Totani et al. 2006; (3) Kashikawa et al. 2006b; (4) This study and Yoshida et al. 2006; Bouwens & Illingworth 2006 and Bouwens et al. 2006; (5) This study and Kobayashi et al. 2007 (K07) model.

formation model in which $f_{\rm esc}^{{\rm Ly}\alpha}$ is not a universal constant but depends on physical conditions of galaxies. This model can reproduce the observed Lyα LF of LAEs at $z\sim3$–6, and predicts that galaxies with strong galaxy-scale outflow, $f_{\rm esc}^{{\rm Ly}\alpha}\sim1$, are dominant in the bright end of Lyα LFs, which is also consistent with observations. It should be noted here that $f_{\rm esc}^{{\rm Ly}\alpha}$ in the K07 model can vary from galaxy to galaxy and may evolve within a galaxy, and hence even if the Lyα photon production rate is proportional to the star formation rate, the evolution of Lyα and UV LFs could be different.

The K07 predictions of the Lyα and UV LFs of LAEs at $z=5.7$, 6.6, and 7 assuming $T_{{\rm Ly}\alpha}^{\rm IGM}=1$ are presented in Figure 7 and 9, respectively. The evolution of number density and Lyα luminosity density of LAEs with a threshold Lyα luminosity predicted by this model are shown in Figure 8. As demonstrated in K07, the deficit of the observed LAEs compared with the model prediction of Lyα LF is clear at $z\gtrsim6$, as seen in Figure 7 while this model precisely reproduces the observed evolution at $z\sim3$–6. On the other hand, the degree of evolution of UVLF of LAEs predicted by the model is similar to that observed in the same redshift range.

The fact that the model prediction is consistent with the UVLF evolution but not with the Lyα LF evolution implies that the evolution of the observed Lyα LF at $z\gtrsim6$ could be caused by IGM absorption. The discrepancy can be resolved if we adopt a simple prescription of luminosity-independent IGM transmission: $T_{{\rm Ly}\alpha}^{\rm IGM}=0.62$–0.78 at $z=6.6$ and $T_{{\rm Ly}\alpha}^{\rm IGM}=0.40$–0.64 at $z=7$.

5.3. *Implications for Reionization*

In the previous section we have shown that the evolution of Lyα LF at $z\gtrsim6$ could be a result of Lyα photon absorption by neutral IGM, implying a significant evolution of the IGM neutral fraction beyond $z\gtrsim6$. In order to obtain some quantitative implications for reionization, however, we must translate the estimates of $T_{{\rm Ly}\alpha}^{\rm IGM}$ obtained in the previous section into the IGM neutral fraction, $x_{\rm H\,I}$. This procedure is not straightforward, because this translation is generally model dependent (e.g., Santos 2004; Dijkstra et al. 2007).

Here, we apply the dynamic model with a reasonable velocity shift of the Lyα line by 360 km s^{-1} redward of the systemic velocity (Santos 2004). The attenuation factor of the Lyα luminosity is given as a function of $x_{\rm H\,I}$; this model is chosen because it predicts no attenuation when $x_{\rm H\,I}=0$. Note that some other models of Santos (2004) predict a significant attenuation even in the case of $x_{\rm H\,I}=0$, due to the neutral gas associated with the host halos of LAEs. Choosing this particular model then means that we ascribe the evolution of the Lyα LF at $z\gtrsim6$ only to absorption by pure IGM. We consider that this is a reasonable assumption, since observations indicate that the escape fraction of Lyα photons is about unity at least for LAEs at $z\sim3$ (Gawiser et al. 2006). If LAEs at $z\sim7$ are a similar population to the low-z LAEs, we do not expect significant absorption by neutral gas physically associated with LAEs. On the other hand, it should also be kept in mind that if $z\sim7$ LAEs are surrounded by a significant amount of nearby neutral gas that is not present for low-z LAEs, the estimate of $x_{\rm H\,I}$ as an average of IGM in the universe could become lower than those derived here.

In § 5.2.2, we obtained $T_{{\rm Ly}\alpha}^{\rm IGM}=0.59$–0.88 and $0.65^{+0.24}_{-0.18}$ at $z=6.6$ and 7.0, respectively. Application of the Santos (2004) model yields the neutral fractions of $x_{\rm H\,I}^{z=6.6}\sim0.12$–0.42 and $x_{\rm H\,I}^{z=7}\sim0.12$–0.54. If we use the K07 model in § 5.2.3 to estimate $x_{\rm H\,I}$, we find $x_{\rm H\,I=0.24-0.36}^{z=6.6}$ from $T_{{\rm Ly}\alpha}^{\rm IGM}=0.62$–0.78 at $z=6.6$, and $x_{\rm H\,I=0.32-0.64}^{z=7}$ from $T_{{\rm Ly}\alpha}^{\rm IGM}=0.40$–0.64 at $z=7$. The neutral fraction $x_{\rm H\,I}$ at $z=6.6$ and 7 estimated from two independent methods is consistent, and tends to increase with redshift at $z>6$. These series of $x_{\rm H\,I}$ values at $z=6.6$ and 7, combined with $x_{\rm H\,I}^{z\sim6.2}\sim0.01$–0.04 and $x_{\rm H\,I}^{z\sim6.3}<0.17$–0.6 derived from quasar GP tests and GRB spectral analysis (Fan et al. 2006; Totani et al. 2006), supports the picture that reionization completed at $z\sim6$, beyond which it was still in progress, with a larger neutral fraction of IGM hydrogen, which evolved with redshift. The neutral IGM fractions obtained by independent methods are summarized in Table 8.

However, our constraint suggests that the neutral IGM persists at the ~50% level as late as $z=7$, and would contradict the *WMAP* conclusion that the reionization epoch is $z=10.9^{+2.7}_{-2.3}$ at the >95% confidence level. Our results could be reconciled with *WMAP* only if there is a statistical fluke (one time in 20, a 95% confidence range is wrong) or if reionization happened twice (e.g., Cen 2003), so that much of the observed electron scattering happened at $z\gg7$, and then the universe became partially neutral again, allowing us to observe neutral gas at $z=7$.

Finally, we again emphasize that these quantitative results are model-dependent and should be interpreted with caution. However, the decrease in the Lyα LF of LAEs beyond $z\sim6$ is more significant than expected from UVLF evolution or a theoretical model, and hence the physical status of the IGM might be changing at $z\gtrsim6$.

6. SUMMARY AND CONCLUSION

We have conducted a narrowband NB973 survey of $z=7$ LAEs, established color criteria to select out $z=7$ LAEs, and found two candidates down to $L({\rm Ly}\alpha)\geq1.0\times10^{43}$ erg s^{-1} (5 σ). By follow-up spectroscopy, the brighter of the two was identified as a $z=6.96$ LAE, while we can confirm neither Lyα emission nor any other features in the spectrum of the other candidate, despite the sufficiently long integration time.

The number and Lyα luminosity densities at $z = 7$ obtained by this study are compared to those at $z = 5.7$ and 6.6 derived from the latest samples obtained by the SDF surveys (Shimasaku et al. 2006; Kashikawa et al. 2006b) down to our detection limit, and clear evolution of density deficits with increasing redshifts was observed, such that $n_{\mathrm{Ly}\alpha}^{z=6.6}/n_{\mathrm{Ly}\alpha}^{z=5.7} \simeq 0.24$ and $n_{\mathrm{Ly}\alpha}^{z=7}/n_{\mathrm{Ly}\alpha}^{z=6.6} \simeq 0.17$; $\rho_{\mathrm{Ly}\alpha}^{z=6.6}/\rho_{\mathrm{Ly}\alpha}^{z=5.7} \simeq 0.21$ and $\rho_{\mathrm{Ly}\alpha}^{z=7}/\rho_{\mathrm{Ly}\alpha}^{z=6.6} \simeq 0.15$. If we assume that the LAE population does not evolve from $z = 7$ to 5.7, this series of density deficits could reflect an increase in neutral IGM hydrogen with redshifts beyond $z \sim 6$.

To see if LAE evolves from $z = 7$ to 6.6, we also compared the UVLF of $z = 7$ LAEs with those of $z = 5.7$ and 6.6 LAEs derived from the SDF LAE surveys. No decrease in the number density of the UVLF was observed from $z = 5.7$ through 6.6 to 7. Since the UV photons are not attenuated by neutral IGM and the UVLF is only sensitive to galaxy evolution, our result suggests that the deficits in $n_{\mathrm{Ly}\alpha}$ and $\rho_{\mathrm{Ly}\alpha}$ might reflect cosmic reionization, and that the LAE population does not significantly evolve at $z = 5.7$–7.

However, the UVLF at $z = 7$ suffers from small statistics, and the interpretation is not robust. Hence, the amount by which the LAE evolution affects the density deficits at $z = 7$, 6.6, and 5.7 was investigated by the inference from the UVLFs of $z < 8$ LBGs (Yoshida et al. 2006; Bouwens & Illingworth 2006; Bouwens et al. 2006) based on the assumption that LAEs evolved in the same way as LBGs, and that the Lyα line luminosities of LAEs are proportional to their UV continuum luminosities. Even after galaxy evolution was taken into account, there still remained some density deficits at these epochs. If we attribute the deficits to the attenuation of Lyα photons by neutral IGM, the neutral fractions of the universe at $z = 6.6$ and 7 are estimated to be 0.12–0.42 and 0.12–0.54, respectively. This result, combined with neutral fractions derived from $z \sim 6$ quasars and a $z \sim 6.3$ GRB, supports the completion of the reionization at $z \sim 6$ and the possible evolution of neutral IGM beyond this redshift.

Again, this result is based on the assumption that LAEs evolved in the same way as LBGs, which might not be the case. Therefore, we also used a LAE evolution model (K07 model) constructed from the hierarchical clustering scenario to reproduce Lyα LFs at $z = 5.7$, 6.6, and 7 in the case of transparent IGM ($x_{\mathrm{H\,I}} = 0$) and compared them with Lyα LFs obtained by the latest SDF surveys (Shimasaku et al. 2006; Kashikawa et al. 2006b; Iye et al. 2006). The observed data at $z = 6.6$ and 7 showed smaller number and luminosity densities than those predicted by the model, suggesting that there still remains the possibility of incomplete reionization at those epochs. The neutral fractions at $z = 6.6$ and 7 estimated from the decline of the LFs by the reionization factors alone after galaxy evolution effects had been corrected are $x_{\mathrm{H\,I}}^{z=6.6} \sim 0.24$–0.36 and $x_{\mathrm{H\,I}}^{z=7} \sim 0.32$–0.64, respectively, also consistent with quasar and GRB results.

The results for $z = 7$ LAE presented here are based on the relatively shallow depth of NB973 imaging, small sample statistics, and only the SDF and optical imaging data. From these data alone, the trend of the density deficit between $z = 5.7$ and 7 in fainter LAE populations and in other places in the universe, changes in physical properties of LAEs associated with their evolution between these epochs, and typical spectroscopic properties of $z = 7$ LAEs, such as the direct detection of the attenuation of the Lyα line, cannot be inferred. In addition, the calculation of the UV continuum flux and thus the UVLF is dependent on relatively rough estimations, without infrared data. Deeper NB973 imaging of the SDF as well as other fields for which infrared images are available and follow-up spectroscopy of newly detected LAE candidates will provide the answers and more precise results in future studies.

We greatly appreciate the technology and engineers of Asahi Spectra Co., Ltd. for developing the NB973 filter that led us to the discovery of the $z = 6.96$ LAE. We are deeply grateful to the staff at the Subaru Telescope for their kind support to make our observations successful. We express gratitude to the SDF team for obtaining and providing us with invaluable imaging data. K. O. acknowledges fellowship support from the Japan Society for the Promotion of Science and the Special Postdoctoral Researchers Program at RIKEN.

REFERENCES

Ajiki, M., et al. 2003, AJ, 126, 2091
Bertin, E., & Arnouts, S. 1996, A&AS, 117, 393
Bouwens, R. J., & Illingworth, G. D. 2006, Nature, 443, 189
Bouwens, R. J., Illingworth, G. D., Blakeslee, J. P., & Franx, M. 2006, ApJ, 653, 53
Brocklehurst, M. 1971, MNRAS, 153, 471
Bruzual, A. G., & Charlot, S. 2003, MNRAS, 344, 1000
Cen, R. 2003, ApJ, 591, 12
Dawson, S., Rhoads, J. E., Malhotra, S., Stern, D., Wang, J., Dey, A., Spinrad, H., & Jannuzi, B. T. 2007, ApJ, 671, 1227
Dijkstra, M., Lidz, A., & Wyithe, J. S. B. 2007, MNRAS, 377, 1175
Fan, X., et al. 2006, AJ, 132, 117
Finkelstein, S. L., Rhoads, J. E., Malhotra, S., Grogin, N., & Wang, J. 2008, ApJ, in press (arXiv:0708.4226)
Furlanetto, S. R., Zaldarriaga, M., & Hernquist, L. 2006, MNRAS, 365, 1012
Gawiser, E., et al. 2006, ApJ, 642, L13
Gehrels, N. 1986, ApJ, 303, 336
Gunn, J. E., & Peterson, B. A. 1965, ApJ, 142, 1633
Haiman, Z., & Spaans, M. 1999, ApJ, 518, 138
Hamuy, M., Suntzeff, N. B., Heathcote, S. R., Walker, A. R., Gigoux, P., & Phillips, M. M. 1994, PASP, 106, 566
Hu, E. M., Cowie, L. L., Capak, P., McMahon, R. G., Hayashino, T., & Komiyama, Y. 2004, AJ, 127, 563
Hu, E. M., Cowie, L. L., McMahon, R. G., Capak, P., Iwamuro, F., Kneib, J.-P., Maihara, T., & Motohara, K. 2002, ApJ, 568, L75
Iye, M., et al. 2006, Nature, 443, 186
Kashikawa, N., et al. 2002, PASJ, 54, 819
———. 2004, PASJ, 56, 1011
Kashikawa, N., et al. 2006a, ApJ, 637, 631
———. 2006b, ApJ, 648, 7
Kennicutt, R. C., Jr. 1998, ARA&A, 36, 189
Kobayashi, M. A. R., Totani, T., & Nagashima, M. 2007, ApJ, 670, 919 (K07)
Kodaira, K., et al. 2003, PASJ, 55, L17
Lehnert, M. D., & Bremer, M. 2003, ApJ, 593, 630
Madau, P. 1995, ApJ, 441, 18
Madau, P., Pozzetti, L., & Dickinson, M. 1998, ApJ, 498, 106
Malhotra, S., & Rhoads, J. E. 2004, ApJ, 617, L5
McQuinn, M., Hernquist, L., Zaldarriaga, M., & Dutta, S. 2007, MNRAS, 381, 75
Miyazaki, S., et al. 2002, PASJ, 54, 833
Nagashima, M., & Yoshii, Y. 2004, ApJ, 610, 23
Oke, J. B. 1990, AJ, 99, 1621
Ouchi, M., et al. 2003, ApJ, 582, 60
———. 2004, ApJ, 611, 660
———. 2005, ApJ, 620, L1
———. 2007, preprint (arXiv:0707.3161)
Page, L., et al. 2007, ApJS, 170, 335
Pirzkal, N., Malhotra, S., Rhoads, J. E., & Xu, C. 2007, ApJ, 667, 49
Rhoads, J. E., & Malhotra, S. 2001, ApJ, 563, L5
Santos, M. R. 2004, MNRAS, 349, 1137
Schechter, P. 1976, ApJ, 203, 297
Sekiguchi, K., et al. 2004, in Multiwavelength Cosmology, ed. M. Plionis (Dordrecht: Kluwer), 169
Sheth, R. K., & Tormen, C. 1999, MNRAS, 308, 119
Shimasaku, K., et al. 2006, PASJ, 58, 313
Somerville, R. S., Lee, K., Ferguson, H. C., Gardner, J. P., Moustakas, L. A., & Giavalisco, M. 2004, ApJ, 600, 171L

Spergel, D. N., et al. 2007, ApJS, 170, 377
Taniguchi, Y., et al. 2005, PASJ, 57, 165
Totani, T., Kawai, N., Kosugi, G., Aoki, K., Yamada, T., Iye, M., Ohta, K., & Hattori, T. 2006, PASJ, 58, 485
Tran, K-.V. H., et al. 2004, ApJ, 612, 89L
van Breukelen, C., Jarvis, M. J., & Venemans, B. P. 2005, MNRAS, 359, 895
Yagi, M., Kashikawa, N., Sekiguchi, M., Doi, M., Yasuda, N., Shimasaku, K., & Okamura, S. 2002, AJ, 123, 66
Yoshida, M., et al. 2006, ApJ, 653, 988